The *Legionella*-driven PtdIns(4)*P* gradient at LCV-ER membrane contact sites promotes Vap-, OSBP- and Sac1-dependent pathogen vacuole remodeling

Simone Vormittag[1], Dario Hüsler[1], Ina Haneburger[1], Tobias Kroniger[2], Aby Anand[3], Manuel Prantl[1], Caroline Barisch[3], Sandra Maaß[2], Dörte Becher[2], François Letourneur[4] & Hubert Hilbi[1*]

[1]Institute of Medical Microbiology, University of Zürich, Gloriastrasse 30, 8006 Zürich, Switzerland.

[2]Institute of Microbiology, University of Greifswald, Felix-Hausdorff-Strasse 8, 17489 Greifswald, Germany.

[3]Division of Molecular Infection Biology and Center for Cellular Nanoanalytics, University of Osnabrueck, Barbarastrasse 13, 49076 Osnabrueck, Germany.

[4]Laboratory of Pathogen Host Interactions, Université de Montpellier, CNRS, INSERM, Place Eugène Bataillon, Montpellier, 34095, cedex 5, France.

Running title: LCV remodeling through ER membrane contact sites

Key words: Amoeba, atlastin, *Dictyostelium discoideum*, large fusion GTPase, host-pathogen interaction, *Legionella pneumophila*, Legionnaires' disease, oxysterol binding protein, pathogen vacuole.

Abbreviations: ATL, Atlastin, FFAT motif, two phenylalanines (FF) in an acidic tract motif; Icm/Dot, intracellular multiplication/defective organelle trafficking; IFC, imaging flow cytometry; LCV, *Legionella*-containing vacuole; GFP, green fluorescent protein; MCS, membrane contact sites; OSBP, oxysterol binding protein; T4SS, type IV secretion system; VAMP, vesicle-associated membrane protein; Vap, VAMP-associated protein.

***Correspondence:** hilbi@imm.uzh.ch; Tel.: +41 (0)44 634 2650

Abstract

The causative agent of Legionnaires' disease, *Legionella pneumophila*, governs interactions with host cells by secreting ca. 330 different "effector" proteins. The facultative intracellular bacteria replicate in macrophages and amoeba within a unique compartment, the *Legionella*-containing vacuole (LCV). Hallmarks of LCV formation are the phosphoinositide (PI) lipid conversion from PtdIns(3)*P* to PtdIns(4)*P*, fusion with endoplasmic reticulum (ER)-derived vesicles and a tight association with the ER. Proteomics of purified LCVs revealed the presence of membrane contact sites (MCS) proteins implicated in lipid exchange. Using dually fluorescence-labeled *Dictyostelium discoideum* amoeba, we reveal that the VAMP-associated protein (Vap), the PtdIns(4)*P* 4-phosphatase Sac1, and the large fusion GTPase Sey1/atlastin-3 localize to the ER, but not to the LCV membrane, and that these ER-resident proteins promote intracellular replication of *L. pneumophila* and LCV remodeling. Moreover, oxysterol binding proteins (OSBPs) preferentially localize to the ER (OSBP8) or the LCV membrane (OSBP11), respectively, and promote (OSBP8) or restrict (OSBP11) intracellular replication of *L. pneumophila* and LCV expansion. Furthermore, the PtdIns(4)*P*-subverting *L. pneumophila* effectors LepB and SidC also promote LCV remodeling. Taken together, the *Legionella*- and host cell-driven PtdIns(4)*P* gradient at LCV-ER MCSs promotes Vap-, OSBP- and Sac1-dependent pathogen vacuole remodeling.

Introduction

Legionella pneumophila is an amoeba-resistant environmental bacterium, which causes a severe pneumonia called Legionnaires' disease [1, 2]. The facultative intracellular pathogen employs a conserved mechanism to grow in free-living protozoa as well as in alveolar macrophages, which is a prerequisite to cause disease [3-6]. To govern the interaction with host cells, *L. pneumophila* employs the Icm/Dot (Intracellular multiplication/defective organelle trafficking) type IV secretion system (T4SS), which translocates ca. 330 different

53 "effector" proteins into host cells [6, 7]. These effector proteins subvert pivotal host cell
54 processes, including the endocytic, secretory, retrograde and autophagy pathways, lipid
55 metabolism, transcription, translation, and apoptosis [8-12].

56 Within host cells, *L. pneumophila* forms a unique, membrane-bound replication
57 compartment, the *Legionella*-containing vacuole (LCV), which restricts interactions with the
58 endocytic pathway [13-16]. Hallmarks of LCV formation are the phosphoinositide (PI) lipid
59 conversion from phosphatidylinositol 3-phosphate (PtdIns(3)*P*) to PtdIns(4)*P*, the subversion
60 of the small GTPase Rab1, fusion of the pathogen vacuole with endoplasmic reticulum (ER)-
61 derived vesicles, and finally, a tight association with the ER [13-16]. The LCV is decorated
62 with PtdIns(4)*P* [17], and PI conversion from the endocytic PI PtdIns(3)*P* to the secretory PI
63 PtdIns(4)*P* occurs in the first 1-2 hours after bacterial uptake [18].

64 The production of PtdIns(4)*P* on the LCV membrane implicates the sequential activity of
65 *L. pneumophila* Icm/Dot-secreted effector proteins: PtdIns 3-kinase MavQ [19], PtdIns(3)*P* 4-
66 kinase LepB [20] and PtdIns(3,4)P_2 3-phosphatase SidF [21]. Moreover, host PI-modulating
67 enzymes such as the PtdIns 4-kinases PI4KIIIα [22] and PI4KIIIβ [23], and the PtdIns(4,5)*P*
68 5-phosphatase OCRL1 [24] might also play a role in the production of PtdIns(4)*P* on the LCV
69 membrane.

70 The small GTPase Rab1 is enriched in the *cis*-Golgi apparatus and controls ER-Golgi
71 secretory trafficking [14]. Rab1 is recruited to the LCV membrane and activated by the
72 Icm/Dot secreted effector SidM (*alias* DrrA), which binds to PtdIns(4)*P* through the novel
73 P4M domain [22, 23, 25-27] and possess Rab1 guanine nucleotide exchange factor (GEF)/
74 guanine dissociation inhibitor (GDI) displacement factor (GDF) activity [28-34] as well as
75 adenosine monophosphorylation (AMPylation) activity [35, 36]. Moreover, Rab1 is de-
76 AMPylated by the effector SidD [37, 38] and reversibly phosphocholinated by the effectors
77 AnkX and Lem3 [39-41]. The covalent modifications of GTP-bound Rab1 lock the small
78 GTPase in its active state. Finally, Rab1 is inactivated by the GTPase activating protein

(GAP) LepB [31]. The small GTPase ARF1 controls also retrograde Golgi-ER trafficking [14]. ARF1 is recruited to and activated on the LCV by the effector RalF, the first *L. pneumophila* GEF identified [42].

The LCV intercepts trafficking at ER exit sites between the ER and the Golgi apparatus, and inhibition of ER-Golgi transport blocks the formation of the pathogen vacuole [42-44]. Sec22b, a SNARE (soluble *N*-ethylmaleimide-sensitive factor (NSF) attachment protein (SNAP) receptor), which promotes fusion of ER-derived vesicles with the *cis*-Golgi, is recruited to LCVs shortly after infection [45, 46]. The activation of Rab1 by SidM on the LCV mediates the fusion of ER-derived vesicles with the pathogen vacuole through the non-canonical pairing of the vesicle (v-)SNARE Sec22b on the vesicles with plasma membrane (PM)-derived target (t-)SNAREs such as syntaxin (Stx) 2, 3, 4 and SNAP23 on the LCV [47, 48]. The LCV intercepts anterograde as well as retrograde trafficking between the ER and the Golgi apparatus [9, 11, 13, 14]. Accordingly, nascent LCVs continuously capture and accumulate PtdIns(4)*P*-positive vesicles from the Golgi apparatus, and their sustained association requires a functional T4SS [49]. LCVs also sequentially recruit the small GTPases Rab33b, Rab6a and the ER-resident SNARE syntaxin18 (Stx18), which are implicated in Golgi-ER retrograde trafficking, to promote the association of the pathogen vacuole with the ER [50].

The association of the LCV with ER in macrophages and amoeba has been initially documented more than 25 years ago [51, 52]. The vacuole containing *L. pneumophila* associates with rough ER within minutes after uptake, and dependent on the Icm/Dot T4SS, the vacuole and the ER form extended contact sites (> 0.5 µm in length), which are connected by tiny, periodic "hair-like" structures [53]. Remarkably, the ER elements remain attached to LCVs even after cell homogenization [53], and intact LCVs purified from *L. pneumophila*-infected *D. discoideum* co-purify with extensive fragments of calnexin-GFP-positive ER [54-56]. In dually fluorescence labeled *D. discoideum*, LCVs accumulate calnexin-positive ER

105 within minutes, and the ER remains separate from the PtdIns(4)*P*-positive pathogen vacuole
106 for at least 8 h post infection [18, 57]. The ER tubules interacting with LCVs are decorated
107 with reticulon 4 (Rtn4) and the large fusion GTPase atlastin/Sey1, which are implicated in the
108 architecture and dynamics of the ER, respectively [58, 59]. The *L. pneumophila* effector Ceg9
109 might stabilize the LCV-ER contact sites by directly binding to the host protein Rtn4 [58].
110 Finally, depletion of the PtdIns(4)*P* 4-phosphatase Sac1, a crucial enzyme of ER membrane
111 contact sites (MCS), reduced the recruitment of endogenous Rab1 to LCVs [22].

112 The MCS between two distinct cellular compartments or organelles adopt a number of
113 functions and are of crucial importance for the non-vesicular exchange of lipids in
114 mammalian cells [60]. MCS between the ER and the PM or organelles promote lipid
115 exchange driven by a gradient of PtdIns(4)*P*, which is established by PtdIns 4-kinases on the
116 PM or organelles and maintained by the integral ER membrane protein PtdIns(4)*P* 4-
117 phosphatase Sac1 [61, 62]. Driven by the PtdIns(4)*P* gradient, phosphatidylserine
118 accumulates at the inner leaflet of the PM [63, 64] and cholesterol accumulates at the Golgi
119 apparatus [61, 65]. The lipid exchange is promoted by lipid transfer proteins termed oxysterol
120 binding proteins (OSBPs), several of which bind PtdIns(4)*P* through a PH domain and by the
121 ER-resident Vap (vesicle-associated membrane protein (VAMP)-associated protein) through a
122 FFAT (two phenylalanines (FF) in an acidic tract) motif [60].

123 Given the accumulation of PtdIns(4)*P* on the limiting LCV membrane and the tight
124 association of the pathogen vacuole with ER, the LCV-ER interface might actually form
125 functionally important MCS, which promote pathogen vacuole remodeling through a
126 PtdIns(4)*P* gradient. Using dually fluorescence-labeled *D. discoideum* amoeba, we identify
127 Vap, Sac1 and Sey1 on the ER, but not on the LCV membrane, while OSBP8 and OSBP11
128 exclusively localize to the ER or the LCV membrane, respectively. The MCS components are
129 implicated in LCV remodeling and intracellular growth of *L. pneumophila*, and a LCV-to-ER
130 PtdIns(4)*P* gradient is established by bacterial effector proteins. These findings indicate that

the *Legionella*-driven PtdIns(4)*P* gradient at LCV-ER MCSs promotes Vap-, Sac1- and OSBP-dependent pathogen vacuole remodeling.

Results

Comparative proteomics of LCVs from *D. discoideum* wild-type and Δ*sey1* reveals MCS components

Given the tight and stable association of the LCV limiting membrane with the ER, MCS are likely formed between the compartments. The ER tubule-resident large GTPase Sey1/Atl3 (DDB_G0279823) promotes the decoration of LCVs with ER, and in absence of the GTPase, significantly less ER accumulates on the pathogen vacuole, while the PtdIns(4)*P*-positive LCV appears to form normally [59, 66]. To gain further insights into the process of LCV formation, and in particular the role of the ER, we analyzed by comparative proteomics LCVs from the *L. pneumophila*-infected *D. discoideum* Ax3 wild-type strain or the Δ*sey1* mutant. This approach revealed 3658 host or bacterial proteins identified on LCVs from *D. discoideum* Ax3 or Δ*sey1* (**Table S1**).

These proteins include the OSBPs OSBP7 (*osbG*) and OSBP8 (*osbH*), the PtdIns(4)*P* 4-phosphatase Sac1, the hydrolase receptor sortilin, the ER proteins calnexin, calmodulin, calreticulin and reticulon, the ER-Golgi intermediate compartment protein-3 (Ergic3), the Golgi proteins golvesin and YIPF1, the vesicle transport through interaction with t-SNAREs homolog 1A (Vti1A), the vesicle-associated membrane protein-7A/B (Vamp7A/B), the vesicle-fusing ATPase (NsfA), the vacuolar protein sorting-associated proteins Vps26, Vps29, and Vps35 (retromer coat complex subunits), dynamin A/B (DymA/B), dynamin-like protein A/C (DlpA/C), Vps4, Vps11, Vps13A, Vps16, Vps45, Vps51, Vps53, syntaxins (5, 7A/B, 8A/B), t-SNAREs, synaptobrevin B, α-SNAP, and many small GTPases or their modulators (Arf1, Arf1 GEF, Arl8, Rab1A/B/C/D, Rab2A/B, Rab4, Rab5A/B, Rab6, Rab7A, Rab8A, Rab11A/C, Rab14, Rab18, Rab21, Rab32A/B/C/D, RabC, RabJ, RabG2, RabQ, Rab GDI,

Rac1A, RacB, RacE, RagA, RanA, RanBP1, RasB, RasC, RasG, RasS, RapA, Rap GAP, Rho GAP, Rho GDI, Sar1, Spg1), as well as the interaptin AbpD [67], the metal ion transporter Nramp1 [68, 69], and the GPCR and receptor protein kinase RpkA [70]. Moreover, many mitochondrial proteins were found to associate with LCVs (**Table S1**). Finally, the *L. pneumophila* PtdIns 4-kinase LepB [20], the PtdIns(4)*P*-binding effectors SidC, its paralogue SdcA, and SidM/DrrA [17, 23, 71], as well as the retromer interactor RidL [72] and the deAMPylase SidD [37, 38] were also identified on LCVs from *D. discoideum* Ax3 and Δ*sey1* (**Table S1**).

Furthermore, 74 *D. discoideum* or 34 *L. pneumophila* proteins were identified only on LCVs from *D. discoideum* Ax3, while 11 host and 3 bacterial proteins were present only on LCVs from Δ*sey1* mutant amoeba (**Fig. 1A**, **Table S1**). Among the host proteins present only on LCVs from *D. discoideum* Ax3, we identified several putative MCS components possibly involved in (PI-driven) lipid transport (OSBP7, Vps13B, CRAL-TRIO domain protein), as well as proteins possibly implicated in ER-Golgi transport (TRAPPC3, YIPF5, γ-SNAP), or localizing to the ER (syntaxin18, calmodulin, Sey1) (**Table S1**). Among the *L. pneumophila* proteins identified only on LCVs from *D. discoideum* Δ*sey1* was the PtdIns(4)*P*-binding effector Lpg2603 [73] (**Table S1**). Based on these findings, we sought to analyze *D. discoideum* factors possibly involved in LCV-ER MCS.

D. discoideum harbors single putative orthologues of the PtdIns(4)*P* 4-phosphatase Sac1 (DDB_G0271630), and the VAMP-associated protein (Vap; DDB_G0278773), as well as several OSBPs, including OSBP7 (DDB_G0283035; *osbG*), OSBP8 (DDB_G0283709; *osbH*) and OSBP11 (DDB_G0288817; *osbK*). All 12 *D. discoideum* OSBPs belong to the class of "short OSBPs", which harbor a putative lipid-binding ORD domain (OSBP-related domain) but lack ankyrin repeats (protein-protein interaction), a PH domain (PI binding), a trans-membrane domain (TMD; membrane interaction), and the FFAT motif (Vap interaction) (**Fig. S1**). OSBP8 and OSBP11 are most similar to one another and most closely related to human

183 short OSBPs. OSBP7 represents an OSBP more distantly related to the other paralogues, and
184 OSBP1 (*osbA*), OSBP2 (*osbB*), OSBP3 (*osbC*), OSBP5 (*osbE*) and OSBP6 (*osbF*) form a
185 separate cluster.

186 In order to validate the localization of MCS components to LCVs, GFP fusion proteins of
187 Vap, OSBP7, OSBP8, OSBP11 or Sac1 were co-produced alongside the PtdIns(4)*P*/LCV
188 probe P4C-mCherry [59] in *D. discoideum* Ax3 or Δ*sey1*, and their localization to LCVs was
189 assessed by imaging flow cytometry (IFC) (**Fig. 1B**). All putative MCS components were
190 found to localize to PtdIns(4)*P*-positive LCVs, and Vap accumulated on significantly fewer
191 LCVs in Δ*sey1* mutant amoeba. Since IFC has a rather low spatial resolution, the PtdIns(4)P-
192 positive limiting LCV membrane cannot be discriminated from tightly associated ER. In
193 summary, comparative proteomics identified MCS components on purified LCVs, the
194 localization of which to the pathogen vacuole was confirmed by IFC.

195

196 ***D. discoideum* MCS components localize to the ER or the LCV membrane**

197 Based on the above bioinformatic and experimental considerations, we sought to analyze the
198 role of the putative MCS components Vap, OSBP7, OSBP8, OSBP11 and Sac1 for LCV
199 formation and the LCV-ER MCS in detail. Using dually fluorescently labeled *D. discoideum*,
200 we assessed by confocal fluorescence microscopy the co-localization of GFP fusions of Vap,
201 OSBP7, OSBP8, OSBP11 or Sac1 with either the ER-resident protein calnexin A-mCherry
202 (CnxA-mCherry), the PtdIns(4)*P*/LCV probe P4C-mCherry, or the endosomal transporter
203 AmtA-mCherry (**Fig. 2A**, **Fig. S2A**). This high-resolution approach revealed that Vap and
204 OSBP8, but significantly less OSBP7 and OSBP11, co-localize with CnxA-mCherry in *L.*
205 *pneumophila*-infected (**Fig. 2B**) as well as in uninfected amoeba (**Fig. S2B-D**). The
206 PtdIns(4)*P* 4-phosphatase Sac1 and its catalytically inactive mutant, Sac1_C383S, also co-
207 localized with CnxA-mCherry, while a Sac1 variant lacking the ER-targeting transmembrane
208 domain, Sac1_ΔTMD, diffusely localized throughout the cell (**Fig. 2B**). Moreover, Vap and

OSBP11 co-localized with P4C-mCherry, while OSBP7, OSBP8 and Sac1 did not (**Fig. 2C**), and Vap and OSBP11 also co-localized with AmtA-mCherry more extensively than the other MCS components (**Fig. 2D**). Finally, OSBP11 intensely localized to the PM. In summary, Vap, OSBP8 and Sac1 co-localize with ER-resident CnxA-mCherry, and Vap as well as OSBP11 co-localize with the PtdIns(4)*P* probe P4C-mCherry and the endosomal/LCV marker AmtA-mCherry (**Table 1**). Hence, at LCV-ER MCS Vap localizes to LCVs as well as to the ER, while OSBP8 and Sac1 preferentially localize to the ER, and OSBP11 preferentially localizes to LCVs.

MCS components modulate the replication of *L. pneumophila* in *D. discoideum* and mammalian cells

To further assess the role of the MCS components for intracellular replication of *L. pneumophila* and LCV formation, we constructed *D. discoideum* deletion mutant strains lacking *vap*, *osbG*, *osbH* or *osbK* by disrupting the corresponding genes with a blasticidin selection marker (**Fig. S3**). Several independent clones of the deletion mutants were picked and further analyzed. Despite repeated attempts, we failed to obtain a Δ*sac1* deletion mutant, and therefore, the gene might be essential in *D. discoideum*. Instead, we constructed and used a dominant negative Sac1 variant lacking the ER-targeting transmembrane domain, Sac1_ΔTMD, and the catalytically inactive Sac1_C383S mutant.

To assess the role of these putative MCS components for intracellular replication of *L. pneumophila*, we used mCherry-producing bacteria and quantified fluorescence intensity (RFU) (**Fig. 3**) and colony forming units (CFU) (**Fig. S4A**). We compared intracellular growth of the wild-type *L. pneumophila* strain JR32 in *D. discoideum* Δ*vap*, as well as in the Δ*osbG*, Δ*osbH*, and Δ*osbK* mutant strains (**Fig. 3A**). In *D. discoideum* Δ*vap*, intracellular bacterial growth was reduced at 4-8 days post infection (p.i.) and enhanced at 10 days p.i. Moreover, intracellular bacterial growth was enhanced in *D. discoideum* Δ*osbH*, reduced in

235 Δ*osbK* and not affected in Δ*osbG*. The intracellular growth phenotypes of *L. pneumophila* in
236 the *D. discoideum* Δ*vap*, Δ*osbH* and Δ*osbK* mutants were reverted by expressing the
237 corresponding genes on a plasmid (**Fig. 3A**). The intracellular growth of *L. pneumophila*
238 strain JR32 was similar in *D. discoideum* Ax3 producing GFP, GFP-Sac1 or GFP-
239 Sac1_C383S but significantly reduced in amoeba producing GFP-Sac1_ΔTMD (**Fig. 3B**, **Fig.**
240 **S4A**). These results are in agreement with the notion that Sac1 is implicated in intracellular
241 growth of *L. pneumophila*, and Sac1_ΔTMD but not GFP-Sac1_C383S interfere with growth
242 in a dominant negative manner. An *L. pneumophila* Δ*icmT* mutant, lacking a functional
243 Icm/Dot T4SS, did not replicate in any of the *D. discoideum* mutant strains (data not shown).
244 Taken together, compared to the parental *D. discoideum* strain, *L. pneumophila* replicates less
245 efficiently in absence of the MCS components Vap or OSBP11 and upon the production of
246 Sac1_ΔTMD, while the bacteria replicate more efficiently in absence of OSBP8 (**Table 1**).
247 OSBPL8 was identified on LCVs purified from *L. pneumophila*-infected RAW 264.7
248 macrophages [55, 56], suggesting that OSBPs and MCS components might also play a role
249 for LCV formation in mammalian cells. To assess the role of MCS components for
250 intracellular replication of *L. pneumophila* in mammalian cells, we used a pharmacological
251 approach and RNA interference. Upon treatment of RAW 264.7 macrophages with the
252 steroidal saponin OSBP inhibitor OSW-1 [65], the intracellular replication of GFP-producing
253 *L. pneumophila* JR32 was significantly inhibited in a dose-dependent manner (**Fig. 3C**).
254 Furthermore, the depletion of Sac1 by RNA interference reduced the intracellular replication
255 of *L. pneumophila* in A549 lung epithelial cells by approximately 25% (**Fig. 3D**, **Fig. S4BC**),
256 similarly to the depletion of the small GTPase Arf1 used as a positive control [59]. Taken
257 together, pharmacological and RNA interference experiments indicate that MCS components
258 also promote the intracellular replication of *L. pneumophila* in mammalian cells.
259

D. discoideum Vap, OSBP11 and Sac1 promote the expansion of PtdIns(4)*P*-positive LCVs

Next, we sought to correlate the intracellular replication of *L. pneumophila* in *D. discoideum* lacking MCS components with alterations of the LCVs. To this end, we quantified the LCV area in *D. discoideum* Ax3 and compared it to the LCVs in the Δ*vap*, Δ*osbG*, Δ*osbH*, Δ*osbK* or Δ*sey1* mutants or to LCVs obtained in strain Ax3 upon production of GFP-Sac1_ΔTMD (**Fig. 4A**, **Fig. S5A**).

Compared to LCVs in *D. discoideum* Ax3, LCVs in the Δ*vap* strain were significantly smaller at 2 h and 8 h p.i., and larger at 16 h p.i. (**Fig. 4B**). Moreover, the LCVs were significantly smaller in the Δ*osbK* mutant strain at 2 h, 8 h and 16 h p.i., larger in the Δ*osbH* mutant at 8 h and 16 h p.i. and did not change in the Δ*osbG* mutant (**Fig. 4B**). Intriguingly, the LCVs in the Δ*osbK* mutant strain were even smaller than in the Δ*sey1* mutant used as a control [66]. The production of GFP-Sac1_ΔTMD in *D. discoideum* Ax3 significantly reduced the LCV size at 2 h, 8 h and 16 h post infection compared to amoeba producing GFP-Sac1 or GFP-Sac1_C383S (**Fig. 4B**). Upon production of GFP-Sac1_ΔTMD in the Δ*vap*, Δ*osbG*, Δ*osbH*, Δ*osbK*, or Δ*sey1* mutant strains the LCV size was also reduced at all time points p.i. compared to amoebae producing GFP-Sac1 (**Fig. S5B**). Taken together, reduced intracellular replication in some *D. discoideum* strains (Δ*vap*, Δ*osbK*, Δ*sey1*, and Sac1_ΔTMD) is positively correlated with a reduced LCV expansion, and increased intracellular replication in the Δ*osbH* mutant is correlated with an enhanced LCV expansion.

Sac1_ΔTMD reduces the accumulation of PtdIns(4)*P*, Vap and OSBP8 on LCV-ER MCS

We then sought to assess the effects of *D. discoideum* MCS components on the LCV PtdIns(4)*P* levels. To this end, we infected amoeba with either mCerulean- or mPlum-

producing *L. pneumophila* and analyzed PtdIns(4)*P* on LCVs by confocal microscopy and imaging flow cytometry (IFC) using dually labeled *D. discoideum* strains producing P4C-mCherry and either GFP-Sac1 (**Fig. 5AB**, **Fig. S6**) or GFP-Sac1_ΔTMD (**Fig. 2A**, **Fig. 4A**, **Fig. 5B**, data not shown).

Compared to the ectopic production of GFP-Sac1, the production of GFP-Sac1_ΔTMD in *D. discoideum* Ax3 resulted in a significant decrease of the IFC P4C colocalization score (see Materials and Methods) for the acquisition of P4C-mCherry on LCV-ER MCV (**Fig. 5B**). GFP-Sac1_ΔTMD localized in strain Ax3 throughout the cell and does not appear to have an organelle preference (**Fig. 2A**, **Fig. 4A**). Accordingly, this result suggests that ectopic production of GFP-Sac1_ΔTMD reduces the PtdIns(4)*P* levels on both the ER as well as the limiting LCV membrane, which cannot be discriminated due to the lower resolution of IFC compared to confocal microscopy. Similarly, the ectopic production of GFP-Sac1_ΔTMD in the *D. discoideum* Δ*vap*, Δ*osbG*, Δ*osbH*, or Δ*osbK* mutant strains resulted in a decrease of PtdIns(4)*P* on LCV-ER MCS (**Fig. 5B**), while GFP-Sac1_ΔTMD localized in the mutant strains throughout the cell (data not shown). At the same time the P4C colocalization score on LCV-ER MCS in the Δ*vap*, Δ*osbG*, Δ*osbH*, or Δ*osbK* mutant strains was similar among the mutants but overall higher than on LCVs in the Ax3 parental strain (**Fig. 5B**). These findings suggest that the depletion of a single MCS component suffices to increase the overall levels of PtdIns(4)*P* on LCV-ER MCS.

Upon production of GFP-Sac1 in the *D. discoideum* Δ*vap*, Δ*osbG*, Δ*osbH*, or Δ*osbK* mutant strains, the IFC Sac1 colocalization score was similar for all LCV-ER MCS (**Fig. 5C**). This result indicates that the localization of Sac1 to LCV-ER MCS is not dependent on Vap or the OSBPs tested. The Sac1 colocalization score was slightly (but not significantly) lower in the Δ*sey1* mutant strain, suggesting that Sey1 might play a role in the acquisition of Sac1 to LCV-ER MCS (**Fig. 5C**). This result is reflected in the finding that Sey1 promotes the

recruitment of ER to LCVs [66]. In summary, compared to the production of GFP-Sac1, the production of GFP-Sac1_ΔTMD in *D. discoideum* Ax3 or the Δ*vap*, Δ*osbG*, Δ*osbH*, Δ*osbK* or Δ*sey1* mutant strains decreased the PtdIns(4)*P* level on LCV-ER MCS, while Sac1 did not change, in agreement with the notion that GFP-Sac1_ΔTMD globally reduces PtdIns(4)*P* levels.

We also assessed by confocal microscopy and IFC the effect of Sac1_ΔTMD for the accumulation of Vap, OSBP7, OSBP8 or OSBP11 on LCVs (**Fig. 5DE**, **Fig. S7**). To this end, we used dually fluorescent labeled *D. discoideum* Ax3 producing either mCherry-Sac1 or mCherry-Sac1_ΔTMD and GFP fusion proteins of Vap, OSBP7, OSBP8 or OSBP11. Compared to the ectopic production of mCherry-Sac1, the production of mCherry-Sac1_ΔTMD in *D. discoideum* Ax3 resulted in a significant decrease of the IFC MCS component colocalization score for the acquisition on LCV-ER MCS of GFP fusions of Vap and OSBP8, but not OSBP7, OSBP11 or Sey1 (**Fig. 5E**). Taken together, compared to the production of mCherry-Sac1, the production of mCherry-Sac1_ΔTMD in *D. discoideum* Ax3, decreased the levels of Vap and OSBP8 on LCV-ER MCS, suggesting that the localization of these MCS components is regulated by PtdIns(4)*P* levels on the LCVs.

The *L. pneumophila* effectors LepB and SidC promote expansion of PtdIns(4)*P*-positive LCVs

To assess the role of *L. pneumophila* effector proteins for LCV remodeling and PtdIns(4)*P* levels, we analyzed LepB, a Rab1 GTPase activating protein (GAP)/PtdIns 4-kinase [20, 31] and SidC, a PtdIns(4)*P* interactor/ubiquitin ligase [17, 57, 74, 75]. To this end, we quantified the LCV area in *D. discoideum* Ax3 producing CnxA-GFP, GFP-Sac1 or GFP-Sac1_ΔTMD, following an infection with mCerulean-producing *L. pneumophila* JR32, Δ*lepB* or Δ*sidC* (**Fig. 6A**, **Fig. S8**).

In *D. discoideum* producing CnxA-GFP, LCVs harboring Δ*lepB* or Δ*sidC* mutant *L. pneumophila* were significantly smaller than LCVs harboring strain JR32 at 1 h, 2 h and 8 h p.i. (**Fig. 6B**). Overall, the LCVs were of similar size in *D. discoideum* producing GFP-Sac1, but significantly smaller in *D. discoideum* producing GFP-Sac1_ΔTMD. In the latter case, LCVs harboring Δ*lepB* or Δ*sidC* mutant *L. pneumophila* were also significantly smaller than LCVs harboring strain JR32 at 1 h, 2 h and 8 h p.i. (Δ*lepB*) and at 1 h p.i. (Δ*sidC*).

In order to correlate the LCV area with the PtdIns(4)*P* levels on the pathogen compartment, we used IFC and *D. discoideum* strains producing in parallel P4C-mCherry and CnxA-GFP, GFP-Sac1 or GFP-Sac1_ΔTMD, infected with mPlum-producing *L. pneumophila* JR32, Δ*lepB* or Δ*sidC* (**Fig. 6C**). In all cases, the IFC colocalization score for the acquisition of P4C-mCherry on LCVs decreased in the course of an infection (1-8 h p.i.). Compared to the parental strain JR32, the score was lowest for Δ*lepB* and intermediate for Δ*sidC*. The colocalization scores were similar in *D. discoideum* producing CnxA-GFP or GFP-Sac1, but significantly lower in *D. discoideum* producing GFP-Sac1_ΔTMD. Taken together, the lack of the *L. pneumophila* Rab1 GAP/PtdIns 4-kinase LepB or the PtdIns(4)*P* interactor/ubiquitin ligase SidC causes a reduction in LCV area and PtdIns(4)*P* levels. These results indicate that the *L. pneumophila* effector proteins LepB and SidC play a role in the PtdIns(4)*P*-dependent LCV remodeling at LCV-ER MCS.

Discussion

In this study, we identified several *D. discoideum* MCS components localizing to LCVs (**Fig. 1**). We then used dually fluorescence-labeled *D. discoideum* amoeba to visualize and quantify MCS components at the LCV-ER interface. The protein Vap localized to the PtdIns(4)*P*-positive LCV membrane as well as the ER, while OSBP8 and Sac1 exclusively localized to the ER, and OSBP11 was detected solely on the LCV membrane (**Fig. 2**, **Table 1**). The MCS

components were found to be implicated in intracellular growth of *L. pneumophila* (**Fig. 3**) and LCV remodeling (**Fig. 4**). Host and bacterial factors regulate the PtdIns(4)*P* levels on LCVs: a derivative of the PtdIns(4)*P* 4-phosphatase Sac1 lacking its membrane anchor, Sac1_ΔTMD (**Fig. 5**), or the lack of the *L. pneumophila* PtdIns 4-kinase, LepB (**Fig. 6**), reduced the PtdIns(4)*P* score on LCVs. Taken together, these findings are compatible with the notion that a *Legionella*- and host cell-driven PtdIns(4)*P* gradient at LCV-ER MCSs promotes Vap-, Sac1- and OSBP-dependent pathogen vacuole remodeling (**Fig. 7**).

We quantified LCV size changes at early infection time points (1-2 h p.i.) to assess the role of MCS components in LCV remodeling (**Fig. 4**, **Fig. 6**). This approach revealed that Vap and even more pronouncedly OSBP11 promote LCV expansion. The size reduction of LCVs in *D. discoideum* Δ*vap* or Δ*osbK* mutant strains was relatively small: the LCVs in the mutant strains were ca. 2-2.5 μm^2, compared to ca. 3 μm^2 in the Ax3 parental strain. Accordingly, these small LCV size changes likely reflect a structural remodeling of the pathogen vacuole rather than a substantial LCV expansion. MCS promote the non-vesicular exchange of lipids in mammalian cells [60], and "counter lipids" transported by OSBPs along a Sac1-dependent PtdIns(4)*P* gradient at ER MCS include phosphatidylserine [63, 64] and cholesterol [61, 65]. The identification of the lipids exchanged by the LCV-ER PtdIns(4)*P* gradient and the specific OSBPs involved will be the subject of future studies.

A massive expansion of the pathogen vacuole at later infection time points (> 8 h p.i.) is required to accommodate intracellular replication of *L. pneumophila* and is likely promoted by vesicle fusion. Indeed, LCV formation implicates the interception of (anterograde and retrograde) vesicular trafficking between the ER and the Golgi apparatus [42-44], and nascent LCVs continuously capture and accumulate PtdIns(4)*P*-positive vesicles from the Golgi apparatus [49]. Further supporting the notion that ER-derived vesicles fuse with LCVs is the finding that the SNARE Sec22b, which promotes fusion of ER-derived vesicles with the *cis*-Golgi, is recruited to LCVs shortly after infection [45, 46]. The fusion requires the *L.*

386 *pneumophila* effector-mediated activation of Rab1 on LCVs and is mediated by the non-
387 canonical pairing of the v-SNARE Sec22b on the vesicles with PM-derived t-SNAREs such
388 as syntaxin2, -3, -4 and SNAP23 on the LCV [47, 48]. In agreement with this scenario,
389 syntaxins (5, 7A/B, 8A/B, 18), t-SNAREs, α- and γ-SNAP as well as Vti1A, Vamp7A/B and
390 NsfA were identified on LCVs by proteomics (**Table S1**).

391 Moreover, several Icm/Dot-translocated *L. pneumophila* effector proteins were identified
392 on LCVs by the comparative proteomics approach (**Table S1**). These effectors prominently
393 include several PtdIns(4)*P*-binding *L. pneumophila* enzymes: the ubiquitin ligase SidC and its
394 paralogue SdcA, the Rab1 GEF/AMPylase SidM/DrrA and the phytate-activated protein
395 kinase Lpg2603. Furthermore, the deAMPylase and SidM antagonist SidD, as well as the
396 retromer interactor RidL were identified on purified LCVs. To study the role of effector
397 proteins for LCV remodeling and PtdIns(4)*P* levels, we analyzed the Δ*lepB* and Δ*sidC* mutant
398 strains (**Fig. 6**). LCVs harboring these mutant strains were smaller and showed a reduced P4C
399 score at LCV-ER MCS. Noteworthy, the effects were augmented in *D. discoideum* producing
400 Sac1_ΔTMD. These results are readily explicable for the PtdIns 4-kinase LepB: if this kinase
401 is lacking, the PtdIns(4)*P* levels on LCVs are lower and LCV remodeling is impaired. The
402 findings are more difficult to interpret for SidC. This effector localizes exclusively on LCVs
403 in *L. pneumophila*-infected *D. discoideum* [54-57] and tightly binds PtdIns(4)*P* with a
404 dissociation constant, K_d, in the range of 240 nM [76]. Hence, SidC might titrate PtdIns(4)*P*
405 levels on LCVs, and its absence in *L. pneumophila* is expected to expose more PtdIns(4)*P* on
406 the pathogen vacuole. Accordingly, the finding that LCVs harboring the Δ*sidC* mutant strain
407 show a lower P4C score is caused by more indirect features of the effector.

408 In addition to the ER-localizing PtdIns(4)*P* 4-phosphatase Sac1, other host cell factors
409 involved in PtdIns(4)*P* turnover might play a role at LCV-ER MCS. The PM-derived PtdIns
410 4-kinase IIIα (PI4KIIIα) [22] and trans-Golgi-derived PI4KIIIβ [23] promote the membrane
411 localization of PtdIns(4)*P*-binding effectors, and therefore, might modulate PtdIns(4)*P* levels

412 on LCVs. Moreover, while the PtdIns(4,5)P_2 5-phosphatase OCRL/Dd5P4 produces
413 PtdIns(4)*P* on LCVs, it restricts intracellular replication of *L. pneumophila* [24, 72],
414 suggesting that this PI phosphatase exerts pleiotropic and complex functions in the context of
415 LCV formation and intracellular bacterial replication.

416 The association of the LCV with ER in amoeba and macrophages represents a
417 longstanding observation [51, 52], which is not understood on a molecular level. In particular,
418 the identity of the tiny, periodic "hair-like" structures between the pathogen vacuole and the
419 ER is unknown. On a similar note, the identity of possible (bacterial or host) tether proteins is
420 not known. A possible candidate for a *L. pneumophila* tether protein is the Icm/Dot-secreted
421 effector Ceg9. This effector might stabilize the LCV-ER contact sites by directly binding to
422 the host protein Rtn4 [58].

423 Several intracellular bacterial pathogens hijack MCS components during infection [77].
424 The mechanistically best characterized case is *Chlamydia trachomatis*, which forms a
425 replication-permissive compartment termed inclusion [77]. Intriguingly, the *Chlamydia*
426 integral membrane proteins IncV and IncD tether the inclusion to the ER [78]. While IncV
427 directly binds Vap on the ER through a FFAT motif [79], IncD indirectly makes contact to
428 Vap through the FFAT motif-containing host protein CERT (ceramide transfer protein) [80,
429 81].

430 Taken together, this study has revealed the importance of host and bacterial factors for
431 MCS formation, LCV remodeling and intracellular replication of *L. pneumophila*. The study
432 paves the way for an in-depth functional and structural analysis of LCV-ER MCS, and future
433 studies will identify possible *L. pneumophila* tethering factors, which promote and stabilize
434 the LCV-ER MCS.

435

436 ## Materials and Methods

437 ### Molecular cloning

438 All plasmids constructed and used are listed in the Supplementary Information (**Table S2**).
439 Cloning was performed using standard protocols, plasmids were isolated by using
440 commercially available kits from Macherey-Nagel, DNA fragments were amplified using
441 Phusion High Fidelity DNA polymerase. For Gibson assembly, the NEBuilder HiFi DNA
442 assembly kit was used. All constructs were verified by DNA sequencing.

443 To construct the knockout vectors for *vap*, *osbG*, and *osbK* (**Table S2**), the corresponding
444 5' fragments were amplified from *D. discoideum* genomic DNA with specific primer pairs
445 oL1277/oL1278, oL1256/oL1356, or oL1687/oL1688, respectively, and cloned into the
446 pBlueScript vector (Stratagene, La Jolla, CA). The 3' fragments were identically produced
447 using the matching primer pairs, oL1279/oL1280, oL1358/oL1359, or oL1693/oL1694,
448 respectively and cloned into pBlueScript containing the 5' fragment. After plasmid sequence
449 verification, the blasticidin resistance cassette was inserted between the two 5'and 3'
450 fragments. The final knockout vectors were digested with KpnI and NotI restriction enzymes
451 before electroporation into Ax3 cells. Blasticidin selection (10 µg/ml) was applied 24 h after
452 transfection. Individual colonies were tested by PCR to confirm gene replacement (**Fig. S3**).
453 The knockout vectors for *osbH* (#629), a kind gift of Prof. Markus Maniak (University of
454 Kassel, Germany), was digested by SpeI and SphI before transfection of Ax3 cells, and
455 transfectants were selected as described above.

456 The *lepB* deletion strain (IH03) was generated essentially as described [83] by double
457 homologous recombination allelic exchange using counter-selection on sucrose (Suc). The 3'
458 and 5' flanking regions of lepB (*lpg2490*) were amplified by PCR using the primer pairs
459 oIH011/oIH013 and oIH012/oIH014, respectively, and genomic *L. pneumophila* DNA as a
460 template. The flanking regions, the Kan^R cassette and the pLAW344 backbone cut with the
461 appropriate restriction enzymes were assembled using a four-way ligation, yielding the
462 suicide plasmid pIH29. *L. pneumophila* JR32 was transformed by electroporation with pIH29,
463 and co-integration of the plasmid was assayed by selection on CYE/Km (5-7 days, 30°C).

Several clones thus obtained were picked and re-streaked on CYE/Km, grown overnight in AYE medium (96-well plates, 180 rpm) and streaked on CYE/Km/2% Suc. After 3-5 days at 37°C, single colonies were spotted on CYE/Cm, CYE/Km/2% Suc and CYE/Km plates to screen for Cm^S, Km^R, Suc^R colonies. Double-cross-over events (deletion mutants) were confirmed by PCR screening and sequencing.

The constructs pMIB39 (*gfp-osbK*), pMIB41 (*gfp-vap*), pMIB87 (*gfp-osbG*), and pMIB89 (*osbH-gfp*) were constructed by PCR amplification using the primers oMIB38/oMIB39, oMIB14/oMIB12, oMIB20/oMIB18 or oMIB21/oMIB22 and cloned into plasmid pDM317 (*osbK*, *vap*, *osbG*) or pDM323 (*osbH*) after digestion with XhoI/SpeI (*osbK*), BamHI/SpeI (*vap*) or BglII/SpeI (*osbG*, *osbH*).

A GFP-Sac1 fusion was constructed by PCR amplification of the putative open reading frame using *D. discoideum* genomic DNA and the primers oLS039 and oLS040 respectively. The DNA fragment was cloned into BglII and SpeI sites of pDM317, yielding pLS037 (GFP-Sac1). The GFP-Sac1 catalytically inactive mutant (Sac1_C383S) was obtained exchanging the codon TGT (cysteine) in position 383 to AGC coding for serine. Nucleotide substitution was carried out by site-directed mutagenesis according to the manufacturer`s recommendation (QuickChange, Agilent) using pLS037 as template and the PAGE purified primers oSV159 and oSV161 yielding pSV015 (GFP-Sac1_C383S). The truncated GFP-Sac1_ΔTMD was obtained by deletion of the transmembrane domain of the *D. discoideum sac1* gene. To this end, pLS037 excluding the transmembrane domain was amplified with the primers oSV227 and oSV228 yielding pSV034. The plasmids pSV044 and pSV045 harboring Sac1 or Sac1_ΔTMD fused to mCherry were constructed by cloning the genes into BglII and SpeI sites of pDM1042. pLS037 and pSV034 were used as templates.

Bacteria, cells, growth conditions, and transformation

Bacterial strains and cell lines used are listed in **Table S2**. *L. pneumophila* strains were grown 3 days on charcoal yeast extract (CYE) agar plates, buffered with *N*-(2-acetamido)-2-aminoethane sulfonic acid (ACES) at 37°C. Liquid cultures in ACES yeast extract (AYE) medium were inoculated at an OD_{600} of 0.1 and grown at 37°C for 21 h to an early stationary phase (2 x 10^9 bacteria/ml). Chloramphenicol (5 µg/ml) was added as required.

D. discoideum stains were grown at 23°C in HL5 medium (ForMedium). Transformation of axenic *D. discoideum* amoeba were performed as described [18, 82]. Blasticidin (10 µg/mL), geneticin (G418, 20 µg/ml) and hygromycin (50 µg/ml) were appropriately added.

Murine macrophage-like RAW 264.7 cells and human A549 lung epithelial carcinoma cells were cultivated in RPMI 1640 medium (Life Technologies) supplemented with 10% heat-inactivated fetal bovine serum (FBS: Life Technologies) and 1% glutamine (Life Technologies). The cells were incubated at 37°C with 5% CO_2 in a humidified atmosphere.

Intracellular replication of *Legionella pneumophila*

Intracellular growth of *L. pneumophila* JR32 and Δ*icmT* in different *D. discoideum* strains was assessed by measuring fluorescence increase during intracellular replication of mCherry-producing *Legionella* strains (relative fluorescence units, RFU) and by determining colony-forming units (CFU).

To determine intracellular replication of mCherry-producing *L. pneumophila*, *D. discoideum* amoebae were seeded (2 × 10^4 cells) in 96-well culture-treated plates (Thermo Fisher) and cultured in HL-5 medium at 23°C. The cells were infected (MOI 1) with the *L. pneumophila* strains JR32 or Δ*icmT* harboring plasmid pNP102. After 21 h growth in AYE medium, the bacteria were diluted in MB medium, centrifuged (450 × *g*, 10 min, RT), and incubated for 1 h at 25°C (well plate was kept moist with water in extra wells). Subsequently, infected cells were washed three times with MB medium, incubated for the time indicated at

514 25°C, and mCherry fluorescence was measured every 2 days using a microtiter plate reader
515 (Synergy H1, Biotek).

516 To assess CFUs, *D. discoideum* amoebae were infected (MOI 1) with mCherry-producing
517 *L. pneumophila* JR32 or Δ*icmT* grown for 21 h, diluted in MB medium, centrifuged and
518 incubated for 1 h at 25°C. The infected cells were washed three times with MB medium and
519 incubated for the time indicated at 25°C. The infected amoebae were lysed for 10 min with
520 0.8% saponin (47036, Sigma-Aldrich). Subsequently, serial dilutions were plated every 2 days
521 on CYE agar plated containing Cam (5 µg/ml) and incubated for 3 days at 37°C. CFUs were
522 counted using an automated colony counter (CounterMat Flash 4000, IUL Instruments,
523 CounterMat software) and the number of CFUs (per ml) was calculated.

524 To test if members of the OSBP family affect intracellular replication of *L. pneumophila* in
525 murine RAW 264.7 macrophages, the steroidal saponin OSBP inhibitor OSW-1 (CAY-30310,
526 Cayman) was added at different concentrations. The macrophages were detached diluted with
527 pre-warmed supplemented RPMI to a concentration of 2.5×10^4 cells/140 µL medium and
528 grown for 24 h in 96-well plates. Liquid cultures of GFP-producing *L. pneumophila* JR32
529 (pNT28) were grown for 21 h and diluted in pre-warmed supplemented RPMI to a
530 concentration of 5×10^4 cells/50 µL medium. A 10 µM OSW-1 stock solution was prepared
531 freshly. Bacterial suspensions, the OSW-1 working solution (final concentration 5, 20 or 100
532 nM) and sterile DPBS were added to wells, yielding an MOI 1. The infection was
533 synchronized by centrifugation (450 × *g*, 10 min.). Plates were incubated at 37°C and 5 %
534 CO_2 in a humidified atmosphere. At the indicated time points (12, 24, 36, 48, 60 h p.i.)
535 intracellular replication was assessed by measuring bacterial GFP production with a plate
536 reader.

537

538 **RNA interference, determination of proteins depletion efficiency and cytotoxicity**

RNA interference experiments were performed as described [59]. Briefly, A549 cells were treated for 48 h with siRNA oligonucleotides with a final concentration of 10 nM in a 96-well plate (RFU) or 24-well plate (toxicity, Western blot) (**Table S3**). The diluted siRNA was added to the wells (5-10 min) at room temperature (RT), and diluted cells (96-well: 2×10^4, 24-well: 6×10^4) in RPMI medium with FBS was added on top (48 h). Subsequently, the cells were infected (MOI 10) with GFP-producing *L. pneumophila* strains (pNT28), centrifuged and incubated for 1 h at 37°C with 5% CO_2, washed three times and incubated for 24 h. GFP fluorescence was measured as described above at 1 h and 24 h post-infection.

Protein depletion efficiency was assessed as follows: cells were harvested in ice-cold PBS and lysed with ice-cold NP-40 cell lysis buffer. Cell extracts were subjected to SDS PAGE. After Western blotting, PVDF membranes were blocked with PBS/5% bovine serum albumin (BSA; Sigma-Aldrich) for 1 h at RT. Subsequently, specific primary antibodies against SacM1L (13033-1-AP, Proteintech) or GAPDH (2118, Cell Signaling) were diluted 1:500 - 1:1,000 in blocking buffer and used to stain the indicated proteins (4°C, overnight). Finally, horse radish peroxidase (HRP)-conjugated secondary antibodies (GE Healthcare Life Sciences) were diluted 1:2,000 in blocking buffer and incubated (1 h, RT). After extensive washing, the enhanced chemiluminescence (ECL) signal was detected with an ImageQuant LAS4000 (GE Healthcare Life Sciences).

To assess cell viability after siRNA treatment, the Zombie Aqua fixable viability kit (BioLegend) was used. A549 cells were grown and treated with siRNA oligonucleotides (**Table S3**) as described above (protein depletion efficiency). Cells treated for 1 h with 70% sterile-filtered ethanol (EtOH) served as positive control for cell death. The cells were then harvested in ice-cold PBS and stained for 30 min in the dark with 50 µl Zombie Aqua dye 1:500 diluted in PBS. Cells were washed once with supplemented RPMI, centrifuged, washed once with PBS, centrifuged and fixed with 4 % paraformaldehyd (PFA) for 30 min at RT. After centrifugation cells were resuspended in 500 µl PBS. Subsequently, cells were subjected

565 to flow cytometry analysis (BD FACS Canto II). Gates were set according to
566 forward/sideward scatter properties, and 10,000 events were collected for each sample. Mean
567 and standard error of mean (SEM) of Zombie-positive cells are shown.
568
569 **Confocal fluorescence microscopy of infected *D. discoideum***
570 Dually fluorescence labeled *D. discoideum* strains were infected, fixed and imaged by
571 confocal fluorescence microscopy. Prior to infection, exponential phase *D. discoideum*
572 amoebae were seeded (1×10^5 cells per well) in HL5 medium containing geneticin (G418,
573 20 µg/ml) and hygromycin (50 µg/ml) in culture treated 6-well plates (VWR) and cultured
574 overnight at 23°C. Cells were infected (MOI 5) with mCerulean-producing *L. pneumophila*
575 JR32 (pNP99), centrifuged (450 × *g*, 10 min, RT) and incubated at 25°C for 1 h.
576 Subsequently, infected cells were washed three times with HL5 medium and incubated at
577 25°C for the time indicated. At given time points, infected cells (including supernatant) were
578 collected from the 6-wells plate, centrifuged (500 × *g*, 5 min, RT) and fixed with 4% PFA
579 (Electron Microscopy Sciences) for 30 min at RT. Following fixation, the cells were washed
580 twice with PBS, transferred to a 16-wells µ-slide dish (Ibidi) and immobilized by adding a
581 layer of PBS/0.5% agarose.
582 Image acquisition was performed using the confocal microscope Leica TCS SP8 X CLSM
583 (HC PL APO CS2, objective 63×/1.4–0.60 oil; Leica Microsystems) with a scanning speed of
584 200 Hz, bi-directional laser scan. Pictures were acquired with a pixel/voxel size close to the
585 instrument's Nyquist criterion of 43 × 43 × 130 nm (xyz). Images were deconvolved with
586 Huygens professional version 19.10 software (Scientific Volume Imaging, http://svi.nl) using
587 the CMLE algorithm, set to 10-20 iterations and quality threshold of 0.05.
588
589 **Imaging flow cytometry of infected *D. discoideum***

590 Processing of infected *D. discoideum* for IFC was performed as described [84, 85]. *D.*
591 *discoideum* cells harboring the plasmids indicated were seeded in a 12-well plate containing
592 HL5 medium, geneticin and hygromycin, and infected (MOI 5) with mPlum-producing *L.*
593 *pneumophila* JR32, Δ*lepB* or Δ*sidC* (pAW014). The infection was synchronized by
594 centrifugation (450 × *g*, 10 min, RT). The cells were incubated for 1 h at 25°C, washed three
595 times with HL5 and incubated at 25°C. At the indicates time points cells were collected,
596 centrifuged (450 × *g*, 5 min, RT) and fixed in 2 % PFA for 90 min on ice. Fixed infected
597 amoebae were washed twice in phosphate-buffered saline (PBS) and resuspended in 20 µl ice
598 cold PBS prior to IFC analysis.
599 At least 5000 cells were acquired using an imaging flow cytometer (ImageStramX MkII;
600 Amnis) and analyzed with the IDEAS (v6.2) software (Amnis). Infected amoeba containing
601 one intracellular *L. pneumophila* bacterium were gated and assessed for colocalization of GFP
602 and mCherry (host) with mPlum produced by the bacteria. The software computes the IFC
603 colocalization score (bright detail similarity), which is the log-transformed Pearson's
604 correlation coefficient of the localized bright spots with a radius of 3 pixels or less in two
605 images and is used to quantify relative enrichment of a marker on the LCV. Data analysis was
606 performed using GraphPad Prism.
607
608 **Comparative proteomics of purified LCVs**
609 LCVs from *D. discoideum* amoebae were purified basically as described [86]. Briefly, *D.*
610 *discoideum* Ax3 or Δ*sey1* producing CnxA-GFP (pAW016) was seeded in T75 flasks (3 per
611 sample) one day before the experiment to reach 80% confluency. The amoebae were infected
612 (MOI 50, 1 h) with *L. pneumophila* JR32 producing mCherry (pNP102) grown to stationary
613 phase (21 h liquid culture). Subsequently, the cells were washed with SorC buffer and scraped
614 in homogenization buffer (20 mM HEPES, 250 mM sucrose, 0.5 mM EGTA, pH 7.2) [45].
615 Cells were homogenized using a ball homogenizer (Isobiotec) with an exclusion size of 8 µm

and incubated with an anti-SidC antibody followed by a secondary anti-rabbit antibody coupled to magnetic beads. The LCVs were separated in a magnetic field and further purified by a density gradient centrifugation step as described [87]. Three independent biological samples were prepared each for LCVs purified from *L. pneumophila*-infected *D. discoideum* Ax3 or Δ*sey1*.

LCVs purified by immuno-magnetic separation and density gradient centrifugation (fraction 4) were resolved by 1D-SDS-PAGE, the gel lanes were excised in ten equidistant pieces and subjected to trypsin digestion [88]. For the subsequent LC-MS/MS measurements, the digests were separated by reversed phase column chromatography using an EASY nLC 1000 (Thermo Fisher Scientific) with self-packed columns (OD 360 µm, ID 100 µm, length 20 cm) filled with 3 µm diameter C18 particles (Dr. Maisch, Ammerbuch-Entringen, Germany) in a one-column setup. Following loading/ desalting in 0.1% acetic acid in water, the peptides were separated by applying a binary non-linear gradient from 5-53% acetonitrile in 0.1% acetic acid over 82 min. The LC was coupled online to a LTQ Orbitrap Elite mass spectrometer (Thermo Fisher, Bremen, Germany) with a spray voltage of 2.5 kV. After a survey scan in the Orbitrap (r = 60,000), MS/MS data were recorded for the twenty most intensive precursor ions in the linear ion trap. Singly charged ions were not considered for MS/MS analysis. The lock mass option was enabled throughout all analyzes.

After mass spectrometric measurement, database search against a database of *Dictyostelium discoideum* and *Legionella pneumophila* Philadelphia downloaded Uniprot on 14/10/2019 (25,478 and 3,024 entries, respectively) as well as label-free quantification (LFQ) was performed using MaxQuant (version 1.6.7.0) (Cox, J and Mann, M (2008). MaxQuant enables high peptide identification rates, individualized p.p.b.-range mass accuracies and proteome-wide protein quantification. Nature Biotechnology 26, 1367–72). Common laboratory contaminants and reversed sequences were included by MaxQuant. Search parameters were set as follows: trypsin/P specific digestion with up to two missed cleavages,

642 methionine oxidation and N-terminal acetylation as variable modification, match between
643 runs with default parameters enabled. The FDRs (false discovery rates) of protein and PSM
644 (peptide spectrum match) levels were set to 0.01. Two identified unique peptides were
645 required for protein identification. LFQ was performed using the following settings: LFQ
646 minimum ratio count 2 considering only unique for quantification.

647 Results were filtered for proteins quantified in at least two out of three biological replicates
648 before statistical analysis. Here, two conditions were compared by a student's t-test applying a
649 threshold p-value of 0.01, which was based on all possible permutations. Proteins were
650 considered to be differentially abundant if the log2-fold change was greater than |0.8|.
651 "ON/OFF proteins" were defined as being identified in all bioreplicates of one strain whereas
652 the protein was not identified in any replicate of the other strain.

653

654 **Statistical methods**

655 Microscopy data analysis was performed using GraphPad Prism. The two-sample Student`s t-
656 test (Mann-Whitnex test, no assumption of Gaussian distributions) was used. Probability
657 values of less than 0.05, 0.01, and 0.001 were used to show statistically significant differences
658 and are represented with *, **, or ***, respectively. The value of "n" represents the number
659 of independent experiments performed or the number of analyzed cells per conditions (**Fig.**
660 **4B**, **Fig. 6B**). For the comparative proteomics, the summarized protein expression values were
661 used for statistical testing of between condition differentially abundant proteins. Empirical
662 Bayes moderated t-tests were applied, as implemented in the R/Bioconductor limma package.

663

664 **Data Availability**

665 The MS proteomics data discussed in this publication have been deposited to the
666 ProteomeXchange Consortium via the PRIDE [89] partner repository with the dataset

667 identifier PXD034490 (Reviewer account details: Username,
668 reviewer_pxd034490@ebi.ac.uk; Password, JrGWYYBQ).
669
670 **Acknowledgements**
671 We would like to thank Markus Maniak for providing the deletion construct for *osbH*, Leoni
672 Swart, Xiaoli Ma, Deise Schäfer, and Iris Hube for help with cloning, and Sebastian Grund
673 for technical support with the preparation of MS samples. Work in the group of H.H. was
674 supported by the Swiss National Science Foundation (SNF; 31003A_175557,
675 310030_207826). Work in the group of D.B. was supported by the Federal Ministry of
676 Education and Research (BMBF; grant 031A410B). Work in the group of C.B. was supported
677 by the DFG and the SFB944 (grant SFB 944/3-P25). Work in the group of F.L. was supported
678 by the Région Occitanie, the Centre National de la Recherche Scientifique (CNRS) and the
679 University of Montpellier (UM). The authors declare no conflict of interest.
680

681 ## References

682 1. Newton HJ, Ang DK, van Driel IR, Hartland EL. Molecular pathogenesis of infections
683 caused by *Legionella pneumophila*. Clin Microbiol Rev. 2010;23(2):274-98.
684 2. Mondino S, Schmidt S, Rolando M, Escoll P, Gomez-Valero L, Buchrieser C.
685 Legionnaires' disease: State of the art knowledge of pathogenesis mechanisms of
686 *Legionella*. Ann Rev Pathol. 2020;15:439-66.
687 3. Hoffmann C, Harrison CF, Hilbi H. The natural alternative: protozoa as cellular models
688 for *Legionella* infection. Cell Microbiol. 2014;16:15-26.
689 4. Boamah DK, Zhou G, Ensminger AW, O'Connor TJ. From many hosts, one accidental
690 pathogen: The diverse protozoan hosts of *Legionella*. Front Cell Infect Microbiol.
691 2017;7:477.

5. Swart AL, Harrison CF, Eichinger L, Steinert M, Hilbi H. *Acanthamoeba* and *Dictyostelium* as cellular models for *Legionella* infection. Front Cell Infect Microbiol. 2018;8:61.
6. Hilbi H, Buchrieser C. Microbe profile: *Legionella pneumophila* - a copycat eukaryote. Microbiology. 2022;168. doi: 10.1099/mic.0.001142.
7. Qiu J, Luo ZQ. *Legionella* and *Coxiella* effectors: strength in diversity and activity. Nat Rev Microbiol. 2017;15:591-605.
8. Finsel I, Hilbi H. Formation of a pathogen vacuole according to *Legionella pneumophila*: how to kill one bird with many stones. Cell Microbiol. 2015;17:935-50.
9. Escoll P, Mondino S, Rolando M, Buchrieser C. Targeting of host organelles by pathogenic bacteria: a sophisticated subversion strategy. Nat Rev Microbiol. 2016;14:5-19.
10. Personnic N, Bärlocher K, Finsel I, Hilbi H. Subversion of retrograde trafficking by translocated pathogen effectors. Trends Microbiol. 2016;24:450-62.
11. Bärlocher K, Welin A, Hilbi H. Formation of the *Legionella* replicative compartment at the crossroads of retrograde trafficking. Front Cell Infect Microbiol. 2017;7:482.
12. Swart AL, Gomez-Valero L, Buchrieser C, Hilbi H. Evolution and function of bacterial RCC1 repeat effectors. Cell Microbiol. 2020;22:e13246.
13. Asrat S, de Jesus DA, Hempstead AD, Ramabhadran V, Isberg RR. Bacterial pathogen manipulation of host membrane trafficking. Ann Rev Cell Dev Biol. 2014;30:79-109.
14. Sherwood RK, Roy CR. Autophagy evasion and endoplasmic reticulum subversion: The Yin and Yang of *Legionella* intracellular infection. Ann Rev Microbiol. 2016;70:413-33.
15. Steiner B, Weber S, Hilbi H. Formation of the *Legionella*-containing vacuole: phosphoinositide conversion, GTPase modulation and ER dynamics. Int J Med Microbiol. 2018;308:49-57.

16. Swart AL, Hilbi H. Phosphoinositides and the fate of *Legionella* in phagocytes. Front Immunol. 2020;11:25.
17. Weber SS, Ragaz C, Reus K, Nyfeler Y, Hilbi H. *Legionella pneumophila* exploits PI(4)*P* to anchor secreted effector proteins to the replicative vacuole. PLoS Pathog. 2006;2(5):e46.
18. Weber S, Wagner M, Hilbi H. Live-cell imaging of phosphoinositide dynamics and membrane architecture during *Legionella* infection. mBio. 2014;5:e00839-13.
19. Li G, Liu H, Luo ZQ, Qiu J. Modulation of phagosome phosphoinositide dynamics by a *Legionella* phosphoinositide 3-kinase. EMBO Rep. 2021;22:e51163.
20. Dong N, Niu M, Hu L, Yao Q, Zhou R, Shao F. Modulation of membrane phosphoinositide dynamics by the phosphatidylinositide 4-kinase activity of the *Legionella* LepB effector. Nat Microbiol. 2016;2:16236.
21. Hsu F, Zhu W, Brennan L, Tao L, Luo ZQ, Mao Y. Structural basis for substrate recognition by a unique *Legionella* phosphoinositide phosphatase. Proc Natl Acad Sci U S A. 2012;109:13567-72.
22. Hubber A, Arasaki K, Nakatsu F, Hardiman C, Lambright D, De Camilli P, et al. The machinery at endoplasmic reticulum-plasma membrane contact sites contributes to spatial regulation of multiple *Legionella* effector proteins. PLoS Pathog. 2014;10:e1004222.
23. Brombacher E, Urwyler S, Ragaz C, Weber SS, Kami K, Overduin M, et al. Rab1 guanine nucleotide exchange factor SidM is a major phosphatidylinositol 4-phosphate-binding effector protein of *Legionella pneumophila*. J Biol Chem. 2009;284:4846-56.
24. Weber SS, Ragaz C, Hilbi H. The inositol polyphosphate 5-phosphatase OCRL1 restricts intracellular growth of *Legionella*, localizes to the replicative vacuole and binds to the bacterial effector LpnE. Cell Microbiol. 2009;11:442-60.

25. Schoebel S, Blankenfeldt W, Goody RS, Itzen A. High-affinity binding of phosphatidylinositol 4-phosphate by *Legionella pneumophila* DrrA. EMBO Rep. 2010;11:598-604.

26. Del Campo CM, Mishra AK, Wang YH, Roy CR, Janmey PA, Lambright DG. Structural basis for PI(4)*P*-specific membrane recruitment of the *Legionella pneumophila* effector DrrA/SidM. Structure. 2014;22:397-408.

27. Hammond GR, Machner MP, Balla T. A novel probe for phosphatidylinositol 4-phosphate reveals multiple pools beyond the Golgi. J Cell Biol. 2014;205:113-26.

28. Machner MP, Isberg RR. Targeting of host Rab GTPase function by the intravacuolar pathogen *Legionella pneumophila*. Dev Cell. 2006;11:47-56.

29. Murata T, Delprato A, Ingmundson A, Toomre DK, Lambright DG, Roy CR. The *Legionella pneumophila* effector protein DrrA is a Rab1 guanine nucleotide-exchange factor. Nat Cell Biol. 2006;8:971-7.

30. Machner MP, Isberg RR. A bifunctional bacterial protein links GDI displacement to Rab1 activation. Science. 2007;318:974-7.

31. Ingmundson A, Delprato A, Lambright DG, Roy CR. *Legionella pneumophila* proteins that regulate Rab1 membrane cycling. Nature. 2007;450:365-9.

32. Suh HY, Lee DW, Lee KH, Ku B, Choi SJ, Woo JS, et al. Structural insights into the dual nucleotide exchange and GDI displacement activity of SidM/DrrA. EMBO J. 2010;29:496-504.

33. Zhu Y, Hu L, Zhou Y, Yao Q, Liu L, Shao F. Structural mechanism of host Rab1 activation by the bifunctional *Legionella* type IV effector SidM/DrrA. Proc Natl Acad Sci U S A. 2010;107:4699-704.

34. Oesterlin LK, Goody RS, Itzen A. Posttranslational modifications of Rab proteins cause effective displacement of GDP dissociation inhibitor. Proc Natl Acad Sci U S A. 2012;109:5621-6.

767 35. Müller MP, Peters H, Blümer J, Blankenfeldt W, Goody RS, Itzen A. The *Legionella*
768 effector protein DrrA AMPylates the membrane traffic regulator Rab1b. Science.
769 2010;329:946-9.
770 36. Hardiman CA, Roy CR. AMPylation is critical for Rab1 localization to vacuoles
771 containing *Legionella pneumophila*. mBio. 2014;5:e01035-13.
772 37. Neunuebel MR, Chen Y, Gaspar AH, Backlund PS, Jr., Yergey A, Machner MP. De-
773 AMPylation of the small GTPase Rab1 by the pathogen *Legionella pneumophila*.
774 Science. 2011;333:453-6.
775 38. Tan Y, Luo ZQ. *Legionella pneumophila* SidD is a deAMPylase that modifies Rab1.
776 Nature. 2011;475:506-9.
777 39. Mukherjee S, Liu X, Arasaki K, McDonough J, Galan JE, Roy CR. Modulation of Rab
778 GTPase function by a protein phosphocholine transferase. Nature. 2011;477:103-6.
779 40. Tan Y, Arnold RJ, Luo ZQ. *Legionella pneumophila* regulates the small GTPase Rab1
780 activity by reversible phosphorylcholination. Proc Natl Acad Sci U S A. 2011;108:21212-
781 7.
782 41. Campanacci V, Mukherjee S, Roy CR, Cherfils J. Structure of the *Legionella* effector
783 AnkX reveals the mechanism of phosphocholine transfer by the FIC domain. EMBO J.
784 2013;32:1469-77.
785 42. Nagai H, Kagan JC, Zhu X, Kahn RA, Roy CR. A bacterial guanine nucleotide exchange
786 factor activates ARF on *Legionella* phagosomes. Science. 2002;295:679-82.
787 43. Kagan JC, Roy CR. *Legionella* phagosomes intercept vesicular traffic from endoplasmic
788 reticulum exit sites. Nat Cell Biol. 2002;4:945-54.
789 44. Robinson CG, Roy CR. Attachment and fusion of endoplasmic reticulum with vacuoles
790 containing *Legionella pneumophila*. Cell Microbiol. 2006;8:793-805.
791 45. Derre I, Isberg RR. *Legionella pneumophila* replication vacuole formation involves rapid
792 recruitment of proteins of the early secretory system. Infect Immun. 2004;72:3048-53.

793 46. Kagan JC, Stein MP, Pypaert M, Roy CR. *Legionella* subvert the functions of rab1 and
794 sec22b to create a replicative organelle. J Exp Med. 2004;199:1201-11.
795 47. Arasaki K, Roy CR. *Legionella pneumophila* promotes functional interactions between
796 plasma membrane syntaxins and Sec22b. Traffic. 2010;11:587-600.
797 48. Arasaki K, Toomre DK, Roy CR. The *Legionella pneumophila* effector DrrA is sufficient
798 to stimulate SNARE-dependent membrane fusion. Cell Host Microbe. 2012;11:46-57.
799 49. Weber S, Steiner B, Welin A, Hilbi H. *Legionella*-containing vacuoles capture
800 PtdIns(4)*P*-rich vesicles derived from the Golgi apparatus. mBio. 2018;9:e02420-18.
801 50. Kawabata M, Matsuo H, Koito T, Murata M, Kubori T, Nagai H, et al. *Legionella* hijacks
802 the host Golgi-to-ER retrograde pathway for the association of Legionella-containing
803 vacuole with the ER. PLoS Pathog. 2021;17:e1009437.
804 51. Swanson MS, Isberg RR. Association of *Legionella pneumophila* with the macrophage
805 endoplasmic reticulum. Infect Immun. 1995;63:3609-20.
806 52. Abu Kwaik Y. The phagosome containing *Legionella pneumophila* within the protozoan
807 *Hartmannella vermiformis* is surrounded by the rough endoplasmic reticulum. Appl
808 Environ Microbiol. 1996;62:2022-8.
809 53. Tilney LG, Harb OS, Connelly PS, Robinson CG, Roy CR. How the parasitic bacterium
810 *Legionella pneumophila* modifies its phagosome and transforms it into rough ER:
811 implications for conversion of plasma membrane to the ER membrane. J Cell Sci.
812 2001;114:4637-50.
813 54. Urwyler S, Nyfeler Y, Ragaz C, Lee H, Mueller LN, Aebersold R, et al. Proteome
814 analysis of *Legionella* vacuoles purified by magnetic immunoseparation reveals secretory
815 and endosomal GTPases. Traffic. 2009;10:76-87.
816 55. Hoffmann C, Finsel I, Otto A, Pfaffinger G, Rothmeier E, Hecker M, et al. Functional
817 analysis of novel Rab GTPases identified in the proteome of purified *Legionella*-
818 containing vacuoles from macrophages. Cell Microbiol. 2014;16:1034-52.

819 56. Schmölders J, Manske C, Otto A, Hoffmann C, Steiner B, Welin A, et al. Comparative
820 proteomics of purified pathogen vacuoles correlates intracellular replication of *Legionella*
821 *pneumophila* with the small GTPase Ras-related protein 1 (Rap1). Mol Cell Proteomics.
822 2017;16:622-41.
823 57. Ragaz C, Pietsch H, Urwyler S, Tiaden A, Weber SS, Hilbi H. The *Legionella*
824 *pneumophila* phosphatidylinositol-4 phosphate-binding type IV substrate SidC recruits
825 endoplasmic reticulum vesicles to a replication-permissive vacuole. Cell Microbiol.
826 2008;10:2416-33.
827 58. Haenssler E, Ramabhadran V, Murphy CS, Heidtman MI, Isberg RR. Endoplasmic
828 reticulum tubule protein reticulon 4 associates with the *Legionella pneumophila* vacuole
829 and with translocated substrate Ceg9. Infect Immun. 2015;83:3479-89.
830 59. Steiner B, Swart AL, Welin A, Weber S, Personnic N, Kaech A, et al. ER remodeling by
831 the large GTPase atlastin promotes vacuolar growth of *Legionella pneumophila*. EMBO
832 Rep. 2017;18:1817-36.
833 60. Pemberton JG, Kim YJ, Balla T. Integrated regulation of the phosphatidylinositol cycle
834 and phosphoinositide-driven lipid transport at ER-PM contact sites. Traffic. 2020;21:200-
835 19.
836 61. Mesmin B, Bigay J, Moser von Filseck J, Lacas-Gervais S, Drin G, Antonny B. A four-
837 step cycle driven by PI(4)P hydrolysis directs sterol/PI(4)P exchange by the ER-Golgi
838 tether OSBP. Cell. 2013;155:830-43.
839 62. Zewe JP, Wills RC, Sangappa S, Goulden BD, Hammond GR. SAC1 degrades its lipid
840 substrate PtdIns4P in the endoplasmic reticulum to maintain a steep chemical gradient
841 with donor membranes. eLife. 2018;7.
842 63. Chung J, Torta F, Masai K, Lucast L, Czapla H, Tanner LB, et al.
843 PI4P/phosphatidylserine countertransport at ORP5- and ORP8-mediated ER-plasma
844 membrane contacts. Science. 2015;349:428-32.

64. Moser von Filseck J, Copic A, Delfosse V, Vanni S, Jackson CL, Bourguet W, et al. Phosphatidylserine transport by ORP/Osh proteins is driven by phosphatidylinositol 4-phosphate. Science. 2015;349:432-6.

65. Mesmin B, Bigay J, Polidori J, Jamecna D, Lacas-Gervais S, Antonny B. Sterol transfer, PI4P consumption, and control of membrane lipid order by endogenous OSBP. EMBO J. 2017;36:3156-74.

66. Hüsler D, Steiner B, Welin A, Striednig B, Swart AL, Molle V, et al. *Dictyostelium* lacking the single atlastin homolog Sey1 shows aberrant ER architecture, proteolytic processes and expansion of the *Legionella*-containing vacuole. Cell Microbiol. 2021:e13318.

67. Rivero F, Kuspa A, Brokamp R, Matzner M, Noegel AA. Interaptin, an actin-binding protein of the alpha-actinin superfamily in *Dictyostelium discoideum*, is developmentally and cAMP-regulated and associates with intracellular membrane compartments. J Cell Biol. 1998;142:735-50.

68. Peracino B, Wagner C, Balest A, Balbo A, Pergolizzi B, Noegel AA, et al. Function and mechanism of action of *Dictyostelium* Nramp1 (Slc11a1) in bacterial infection. Traffic. 2006;7:22-38.

69. Buracco S, Peracino B, Cinquetti R, Signoretto E, Vollero A, Imperiali F, et al. *Dictyostelium* Nramp1, which is structurally and functionally similar to mammalian DMT1 transporter, mediates phagosomal iron efflux. J Cell Sci. 2015;128:3304-16.

70. Riyahi TY, Frese F, Steinert M, Omosigho NN, Glockner G, Eichinger L, et al. RpkA, a highly conserved GPCR with a lipid kinase domain, has a role in phagocytosis and anti-bacterial defense. PLoS One. 2011;6:e27311.

71. Luo ZQ, Isberg RR. Multiple substrates of the *Legionella pneumophila* Dot/Icm system identified by interbacterial protein transfer. Proc Natl Acad Sci U S A. 2004;101:841-6.

870 72. Finsel I, Ragaz C, Hoffmann C, Harrison CF, Weber S, van Rahden VA, et al. The
871 *Legionella* effector RidL inhibits retrograde trafficking to promote intracellular
872 replication. Cell Host Microbe. 2013;14:38-50.
873 73. Sreelatha A, Nolan C, Park BC, Pawlowski K, Tomchick DR, Tagliabracci VS. A
874 *Legionella* effector kinase is activated by host inositol hexakisphosphate. J Biol Chem.
875 2020.
876 74. Hsu F, Luo X, Qiu J, Teng YB, Jin J, Smolka MB, et al. The *Legionella* effector SidC
877 defines a unique family of ubiquitin ligases important for bacterial phagosomal
878 remodeling. Proc Natl Acad Sci U S A. 2014;111:10538-43.
879 75. Luo X, Wasilko DJ, Liu Y, Sun J, Wu X, Luo ZQ, et al. Structure of the *Legionella*
880 virulence factor, SidC reveals a unique PI(4)*P*-specific binding domain essential for its
881 targeting to the bacterial phagosome. PLoS Pathog. 2015;11:e1004965.
882 76. Dolinsky S, Haneburger I, Cichy A, Hannemann M, Itzen A, Hilbi H. The *Legionella*
883 *longbeachae* Icm/Dot substrate SidC selectively binds phosphatidylinositol 4-phosphate
884 with nanomolar affinity and promotes pathogen vacuole-endoplasmic reticulum
885 interactions. Infect Immun. 2014;82:4021-33.
886 77. Derre I. Hijacking of membrane contact sites by intracellular bacterial pathogens. Adv
887 Exp Med Biol. 2017;997:211-23.
888 78. Stanhope R, Derre I. Making contact: VAP targeting by intracellular pathogens. Contact.
889 2018;1. doi: 10.1177/2515256418775512.
890 79. Stanhope R, Flora E, Bayne C, Derre I. IncV, a FFAT motif-containing *Chlamydia*
891 protein, tethers the endoplasmic reticulum to the pathogen-containing vacuole. Proc Natl
892 Acad Sci U S A. 2017;114:12039-44.
893 80. Derre I, Swiss R, Agaisse H. The lipid transfer protein CERT interacts with the
894 *Chlamydia* inclusion protein IncD and participates to ER-*Chlamydia* inclusion membrane
895 contact sites. PLoS Pathog. 2011;7:e1002092.

81. Elwell CA, Jiang S, Kim JH, Lee A, Wittmann T, Hanada K, et al. *Chlamydia trachomatis* co-opts GBF1 and CERT to acquire host sphingomyelin for distinct roles during intracellular development. PLoS Pathog. 2011;7:e1002198.

82. Weber S, Hilbi H. Live cell imaging of phosphoinositide dynamics during *Legionella* infection. Methods Mol Biol. 2014;1197:153-67.

83. Tiaden A, Spirig T, Weber SS, Brüggemann H, Bosshard R, Buchrieser C, et al. The *Legionella pneumophila* response regulator LqsR promotes host cell interactions as an element of the virulence regulatory network controlled by RpoS and LetA. Cell Microbiol. 2007;9:2903-20.

84. Welin A, Weber S, Hilbi H. Quantitative imaging flow cytometry of *Legionella*-infected *Dictyostelium* amoebae reveals the impact of retrograde trafficking on pathogen vacuole composition. Appl Environ Microbiol. 2018;84:e00158-18.

85. Welin A, Weber S, Hilbi H. Quantitative imaging flow cytometry of *Legionella*-containing vacuoles in dually fluorescence-labeled *Dictyostelium*. Methods Mol Biol. 2019;1921:161-77.

86. Urwyler S, Finsel I, Ragaz C, Hilbi H. Isolation of *Legionella*-containing vacuoles by immuno-magnetic separation. Curr Prot Cell Biol. 2010;Chapter 3, unit 3 34.

87. Hoffmann C, Finsel I, Hilbi H. Pathogen vacuole purification from *Legionella*-infected amoeba and macrophages. Methods Mol Biol. 2013;954:309-21.

88. Bonn F, Bartel J, Buttner K, Hecker M, Otto A, Becher D. Picking vanished proteins from the void: how to collect and ship/share extremely dilute proteins in a reproducible and highly efficient manner. Anal Chem. 2014;86:7421-7.

89. Perez-Riverol Y, Csordas A, Bai J, Bernal-Llinares M, Hewapathirana S, Kundu DJ, et al. The PRIDE database and related tools and resources in 2019: improving support for quantification data. Nucleic Acids Res. 2019;47:D442-D50.

Table 1. Features of selected *D. discoideum* MCS components.

	Colocalization			*Legionella* Icm [a]
MCS component	Calnexin (ER) [a]	P4C (PI4*P*/LCV) [a]	AmtA (PM/EE) [a]	
Vap	++	++	+	positive
OSBP7 (*osbG*)	++/- [b]	-	-	no effect
OSBP8 (*osbH*)	++	-	-	negative
OSBP11 (*osbK*)	-	++	++	positive
Sac1	++	-	-	no effect
Sac1_C383S	++	-	-	no effect
Sac1_ΔTMD	-	-	-	negative

[a] Abbreviations: Icm, intracellular multiplication of *L. pneumophila* in *D. discoideum* producing the Sac1 variants or lacking *vap*, *osbG*, *osbH* or *osbK*, compared to replication in the parental strain Ax3; ER, endoplasmic reticulum; EE, early endosome; PI4*P*/LCV, phosphatidylinositol 4-phosphate/*Legionella*-containing vacuole; PM, plasma membrane.

[b] +: co-localization in *L. pneumophil*a-infected cells; -: no co-localization in uninfected cells.

928 **Figure Legends**

929 **Figure 1.** *D. discoideum* MCS components localizing to LCVs.

930 (**A**) Comparative proteomics was performed by mass spectrometry with LCVs purified from
931 *L. pneumophila*-infected *D. discoideum* Ax3 or Δ*sey1* (for details see Materials and Methods).
932 Among the total of 3658 eukaryotic or bacterial proteins identified, the Venn diagrams show
933 proteins identified in biological triplicates only on LCVs from *D. discoideum* Ax3 (108
934 proteins; 74 *D. discoideum*, 34 *L. pneumophila*) or only on LCVs from Δ*sey1* mutant amoeba
935 (14 proteins; 11 *D. discoideum*, 3 *L. pneumophila*). (**B**) Imaging flow cytometry (IFC) of *D.*
936 *discoideum* Ax3 or or Δ*sey1* producing P4C-mCherry (pWS032) and GFP fusion proteins of
937 Vap, OSBP7, OSBP8, OSBP11, or Sac1, infected (MOI 5, 1 h) with mPlum-producing *L.*
938 *pneumophila* JR32 (pAW014). Mean IFC colocalization score and standard error of mean
939 (SEM) for MCS component GFP fusion proteins for > 5000 LCVs is depicted. The data are
940 representative for three independent experiments (***P<0.001).

941

942 **Figure 2.** *Dictyostelium discoideum* MCS components localize to LCVs and/or ER.

943 (**A**) Dually labeled *D. discoideum* amoebae producing MCS components fused to GFP, and
944 either calnexin (CnxA)-mCherry (pAW012), P4C-mCherry (pWS032), or AmtA-mCherry
945 were infected (MOI 5, 2 h) with mCerulean-producing *L. pneumophila* JR32 (pNP99), fixed
946 with 4 % PFA, and imaged by confocal fluorescence microscopy. Merged images are shown.
947 Scale bars: 3 µm. The Pearson's correlation coefficient was generated using Coloc 2 from Fiji
948 (ImageJ) and is shown for MCS components fused to GFP with respect to (**B**) CnxA-
949 mCherry, (**C**) P4C-mCherry, or (**D**) AmtA-mCherry.

950

951 **Figure 3.** MCS components modulate replication of *Legionella pneumophila* in *Dictyostelium*
952 *discoideum* and mammalian cells.

(**A**) *D. discoideum* Ax3, or the Δ*vap*, Δ*osbG,* Δ*osbH*, or Δ*osbK* mutant strains producing GFP (pDM317) or GFP fusions of the MCS components were infected (MOI 1) with mCherry-producing *L. pneumophila* JR32 (pNP102), and intracellular replication was assessed by relative fluorescence units (RFU). Mean and SEM of three independent experiments are shown (*P<0.05; **P<0.01; ***P<0.001). (**B**) *D. discoideum* Ax3 producing CnxA-GFP (pAW016), GFP-Sac1 (pLS037), GFP-Sac1_C383S (pSV015) or GFP-Sac1_ΔTMD (pSV034) were infected (MOI 1) with mCherry-producing *L. pneumophila* JR32 (pNP102), and intracellular replication was assessed by relative fluorescence units (RFU). Mean and SEM of three independent experiments are shown (***P<0.001). (**C**) RAW 264.7 macrophages were treated with increasing concentrations of OSW-1 (0-100 nM, 1-60 h), infected (MOI 1) with GFP-producing *L. pneumophila* JR32 (pNT28), and intracellular replication was assessed by relative fluorescence units (RFU). Mean and SEM of three independent experiments are shown (*P<0.05; ***P<0.001). (**D**) A549 epithelial cells transfected for 48 h with 10 nM siRNA oligonucleotides were infected (MOI 10) with GFP-producing *L. pneumophila* JR32 or Δ*icmT* (pNT28), and intracellular replication was assessed by fluorescence with a microplate reader. Growth after 24 h was compared to growth at 1 h. Mean and SEM of three independent experiments are shown (**P<0.01).

Figure 4. Vap, OSBP11, and Sac1 promote expansion of PtdIns(4)*P*-positive LCVs.

(**A**) Dually labeled *D. discoideum* Ax3, Δ*vap*, Δ*osbG,* Δ*osbH*, Δ*osbK* or Δ*sey1* mutants producing P4C-mCherry (pWS032) and CnxA-GFP (pAW016), or Ax3 producing P4C-mCherry and either GFP-Sac1 (pLS037), GFP-Sac1_C383S (pSV015) or GFP-Sac1_ΔTMD (pSV034) were infected (MOI 5, 2-16 h) with mCerulean-producing *L. pneumophila* JR32 (pNP99) and fixed with 4 % PFA. Merged images for the analyzed time points are shown. Scale bars: 3 µm. (**B**) LCV area was measured using ImageJ (n=100-200 per condition from 3

978 independent biological replicates). Means and SEM of single cells are shown (**P<0.01;
979 ***P<0.001).
980
981 **Figure 5.** Sac1_ΔTMD reduces the accumulation of PtdIns(4)*P*, Vap and OSBP8 on LCVs.
982 (**A**) Dually labeled *D. discoideum* Ax3, Δ*vap*, Δ*osbG,* Δ*osbH*, Δ*osbK* or Δ*sey1* mutants
983 producing P4C-mCherry (pWS032) and GFP-Sac1 (pLS037) were infected (MOI 5, 2-16 h)
984 with mCerulean-producing *L. pneumophila* JR32 (pNP99) and fixed with 4 % PFA. Merged
985 images for the analyzed time points are shown. Scale bars: 3 µm. (**B**, **C**) Imaging flow
986 cytometry (IFC) analysis of dually labeled *D. discoideum* Ax3, Δ*vap*, Δ*osbG,* Δ*osbH*, Δ*osbK*
987 or Δ*sey1* mutants producing P4C-mCherry (pWS032) and either GFP-Sac1 (pLS037) or GFP-
988 Sac1_ΔTMD (pSV034), infected (MOI 5, 2 h) with mPlum-producing *L. pneumophila* JR32
989 (pAW014). (**D**) Dually labeled *D. discoideum* Ax3 producing GFP fusions of MCS
990 components and either mCherry-Sac1 (pSV044) or mCherry-Sac1_ΔTMD (pSV045) were
991 infected (MOI 5, 2 h) with mCerulean-producing *L. pneumophila* JR32 (pNP99) and fixed
992 with 4 % PFA. Merged images for the analyzed time points are shown. Scale bars: 3 µm. (**E**)
993 IFC analysis of dually labeled *D. discoideum* Ax3 producing GFP fusions of MCS
994 components and either mCherry-Sac1 (pSV044) or mCherry-Sac1_ΔTMD (pSV045), infected
995 (MOI 5, 2 h) with mPlum-producing *L. pneumophila* JR32 (pAW014). Quantification of (B)
996 P4C-mCherry (C) Sac1-GFP or (E) GFP fusions of MCS components localizing to LCVs at 2
997 h p.i. Due to the lower resolution of IFC, "LCVs" designates the LCV limiting membrane and
998 tightly attached ER. Number of events per sample, n = 5000. Data represent mean and SEM
999 of three independent experiments (*P<0.05; **P<0.01; ***P<0.001).
1000
1001 **Figure 6.** The *L. pneumophila* effectors LepB and SidC determine PtdIns(4)*P* decoration and
1002 expansion of LCVs.

(**A**) Dually labeled *D. discoideum* Ax3 producing P4C-mCherry (pWS032) and either CnxA-GFP (pAW016), GFP-Sac1 (pLS037), or GFP-Sac1_ΔTMD (pSV034) were infected (MOI 5, 1-8 h) with mCerulean-producing *L. pneumophila* JR32, Δ*lepB* or Δ*sidC* (pNP99) and fixed with 4 % PFA. Merged images for the analyzed time points are shown. Scale bars: 3 µm. (**B**) LCV area was measured using ImageJ (n=100-200 per condition). Means and SEM of single cells are shown (**P<0.01; ***P<0.001). (**C**) Imaging flow cytometry (IFC) analysis of dually labeled *D. discoideum* Ax3 producing P4C-mCherry (pWS032) and either CnxA-GFP (pAW016), GFP-Sac1 (pLS037), or GFP-Sac1_ΔTMD (pSV034), infected (MOI 5, 1-8 h) with mPlum-producing *L. pneumophila* JR32 (pAW014). Number of events per sample, n = 5000. Data represent mean and SEM of three independent experiments (*P<0.05; **P<0.01; ***P<0.001).

Figure 7. Localization and function of host and bacterial factors at LCV-ER MCS.
In dually fluorescence-labeled *D. discoideum* amoeba MCS components such as Vap, OSBPs and Sac1 localize to the LCV-ER interface. The host proteins Vap, OSBP8, Sac1 and Sey1 localize to the ER, and OSBP11 is detected on the PtdIns(4)*P*-positive LCV membrane as well as on the PM. The MCS components are implicated in intracellular growth of *L. pneumophila* and LCV remodeling. The PtdIns(4)*P* 4-phosphatase Sac1 lacking its membrane anchor, Sac1_ΔTMD, or the lack of the *L. pneumophila* PtdIns(3)*P* 4-kinase, LepB, reduced the PtdIns(4)*P* score on LCV-ER MCS. These findings suggest that a *Legionella*- and host cell-driven PtdIns(4)*P* gradient at LCV-ER MCS promotes Vap-, OSBP- and Sac1-dependent pathogen vacuole remodeling.

Supplementary Figures

Figure S1. Phylogenetic tree of short OSBPs from *D. discoideum*, *Saccharomyces cerevisiae* and humans.

Sequences of all proteins were either derived from dictybase.org or uniprot and aligned with MAFFT (https://mafft.cbrc.jp) using the G-INS-I strategy, unalignlevel 0.8 and "leave gappy regions" to generate a phylogenetic tree in phylo.ilo using NJ conserved sites and the JTT substitution model. Numbers on the branches indicate bootstrap support for nodes from 100 bootstrap replicates.

Figure S2. *Dictyostelium discoideum* MCS components localize to LCVs and/or ER.

(**A**) Dually labeled *D. discoideum* amoebae producing MCS components fused to GFP and either CnxA-mCherry (pAW016), P4C-mCherry (pWS032), or AmtA-mCherry were infected (MOI 5, 2 h) with mCerulean-producing *L. pneumophila* JR32 (pNP99), fixed with 4 % PFA, and imaged by confocal fluorescence microscopy. Single channels are shown. scale bars: 3 µm. The Pearson's correlation coefficient of uninfected cells was generated using Coloc 2 from Fiji (ImageJ) and is shown for MCS components fused to GFP with respect to (**B**) CnxA-mCherry, (**C**) P4C-mCherry, or (**D**) AmtA-mCherry. Data represent mean and SEM of three independent experiments (*P<0.05; ***P<0.001).

Figure S3. Construction of *D. discoideum* deletion mutants.

Schematic representation of the strategies followed for the construction of *D. discoideum* strains lacking (**A**) *osbG*, (**B**) *osbH*, (**C**) *osbK*, or (**D**) *vap*, and PCR-based validation.

Figure S4. MCS components modulate replication of *L. pneumophila* in *D. discoideum* and mammalian cells.

(**A**) *D. discoideum* Ax3, or Δ*vap*, Δ*osbG,* Δ*osbH*, or Δ*osbK* mutants producing GFP-Sac1 (pLS037) or GFP-Sac1_ΔTMD (pSV034) were infected (MOI 1) with mCherry-producing *L. pneumophila* JR32 (pNP102), and intracellular replication was assessed by colony-forming units (CFU). Mean and SEM of three independent experiments are shown (*P<0.05;

P<0.01; ***P<0.001). To improve clarity, the different mutant strains are shown in separate graphs, each depicting the same data for Ax3/GFP-Sac1. (B**) Cytotoxicity toward A549 cells of oligonucleotides targeting Arf1 and Sac1 (10 nM siRNA, 48 h) was determined by the Zombie Aqua fixable viability kit (BioLegend) using flow cytometry. Percentage of Zombie-positive cells is shown (means and SEM of triplicate experiments). Untreated cells were used as a negative control, and treatment with 70% EtOH for 1 h served as positive control for cell death. (**C**) A549 epithelial cells were treated with oligonucleotides targeting Sac1 (10 nM siRNA, 48 h), and the efficiency of protein depletion was assessed by Western blot (WB) with the antibodies indicated. Qiagen AllStars unspecific oligonucleotides ("Scrambled", "Scr") were used to control for off-target effects, and GAPDH served as WB loading control. Data are representative of two independent experiments.

Figure S5. Vap, OSBP11, and Sac1 promote expansion of PtdIns(4)*P*-positive LCVs.

Dually labeled *D. discoideum* Ax3, Δ*vap*, Δ*osbG,* Δ*osbH*, Δ*osbK* or Δ*sey1* mutants producing P4C-mCherry (pWS032) and CnxA-GFP (pAW016), or Ax3 producing P4C-mCherry and either GFP-Sac1 (pLS037), GFP-Sac1_C383S (pSV015) or GFP-Sac1_ΔTMD (pSV034) were infected (MOI 5, 2-16 h) with mCerulean-producing *L. pneumophila* JR32 (pNP99) and fixed with 4 % PFA. Single channels for the analyzed time points are shown. Scale bars: 3 µm.

Figure S6. Localization of GFP-Sac1 in *D. discoideum* Ax3 or strains lacking MCS components.

Dually labeled *D. discoideum* Ax3, Δ*vap*, Δ*osbG,* Δ*osbH*, Δ*osbK* or Δ*sey1* mutants producing P4C-mCherry (pWS032) and GFP-Sac1 (pLS037) were infected (MOI 5, 2-16 h) with mCerulean-producing *L. pneumophila* JR32 (pNP99) and fixed with 4 % PFA. Single channels for the analyzed time points are shown. Scale bars: 3 µm.

Figure S7. Localization of GFP-MCS components in *D. discoideum* wild-type producing Sac1 or Sac1_ΔTMD.

Dually labeled *D. discoideum* Ax3 producing GFP fusions of MCS proteins and either mCherry-Sac1 (pSV044) or mCherry-Sac1_ΔTMD (pSV045) were infected (MOI 5, 2 h) with mCerulean-producing *L. pneumophila* JR32 (pNP99) and fixed with 4 % PFA. Single channels for the analyzed time points are shown. Scale bars: 3 µm.

Figure S8. The *L. pneumophila* effectors LepB and SidC determine PtdIns(4)*P* decoration and expansion of LCVs.

Dually labeled *D. discoideum* Ax3 producing P4C-mCherry (pWS032) and either CnxA-GFP (pAW016), GFP-Sac1 (pLS037), or GFP-Sac1_ΔTMD (pSV034) were infected (MOI 5, 1-8 h) with mCerulean-producing *L. pneumophila* JR32, Δ*lepB* or Δ*sidC* (pNP99) and fixed with 4 % PFA. Single channels for the analyzed time points are shown. Scale bars: 3 µm.

Table S1. Comparative proteomics of LCVs from *D. discoideum* Ax3 and Δ*sey1*.

Table S2. Cells, bacterial strains, and plasmids used in this study.

Table S3. Oligonucleotides used in this study.

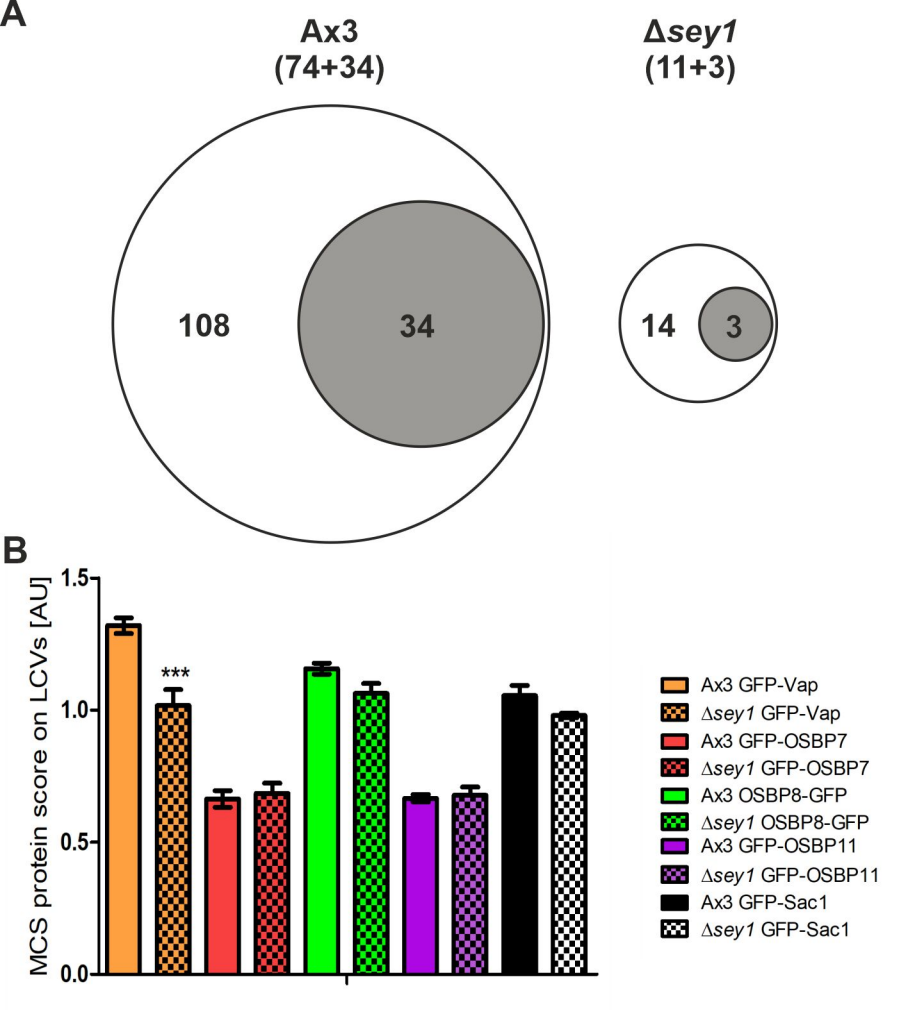
A
Ax3
(74+34)
Δsey1
(11+3)
108
34
14
3
B
MCS protein score on LCVs [AU]
1.5
1.0
0.5
0.0
***
Ax3 GFP-Vap
Δsey1 GFP-Vap
Ax3 GFP-OSBP7
Δsey1 GFP-OSBP7
Ax3 OSBP8-GFP
Δsey1 OSBP8-GFP
Ax3 GFP-OSBP11
Δsey1 GFP-OSBP11
Ax3 GFP-Sac1
Δsey1 GFP-Sac1

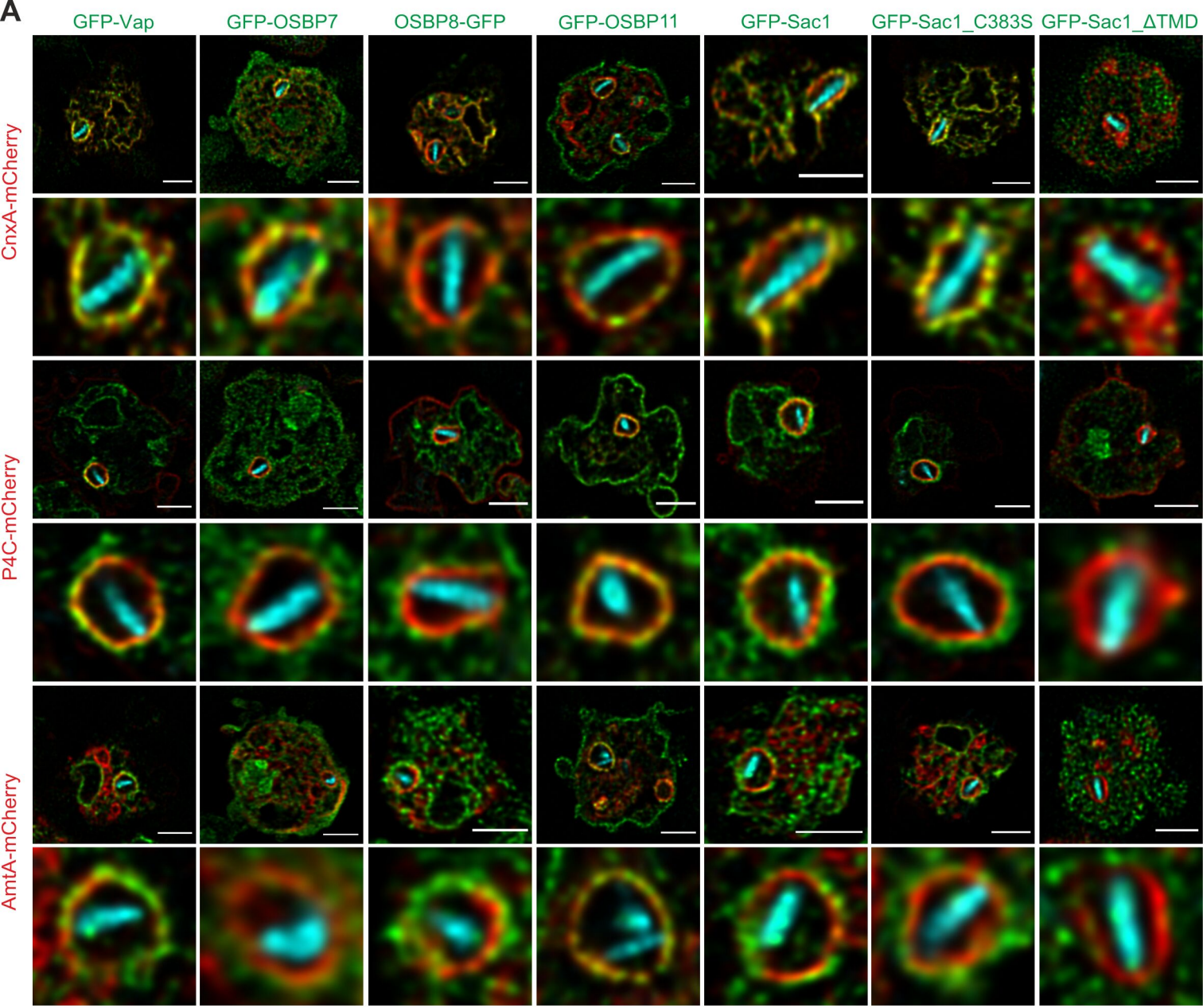
A
GFP-Vap
GFP-OSBP7
OSBP8-GFP
GFP-OSBP11
GFP-Sac1
GFP-Sac1_C383S
GFP-Sac1_ΔTMD
CnxA-mCherry
P4C-mCherry
AmtA-mCherry

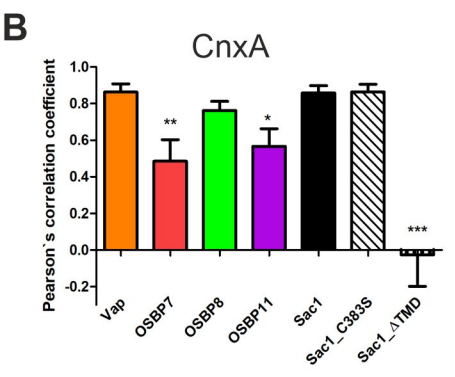
B
CnxA
Pearson`s correlation coefficient
1.0
0.8
0.6
0.4
0.2
0.0
-0.2
**
*
***
Vap
OSBP7
OSBP8
OSBP11
Sac1
Sac1_C383S
Sac1_ΔTMD

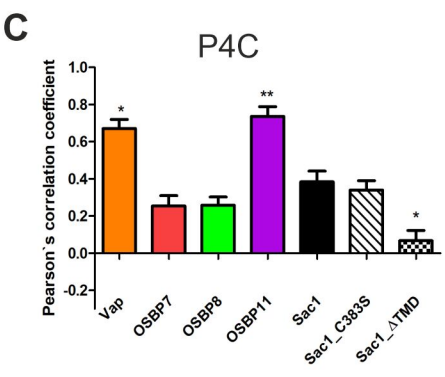
C
P4C
Pearson`s correlation coefficient
1.0
0.8
0.6
0.4
0.2
0.0
-0.2
*
**
*
Vap
OSBP7
OSBP8
OSBP11
Sac1
Sac1_C383S
Sac1_ΔTMD

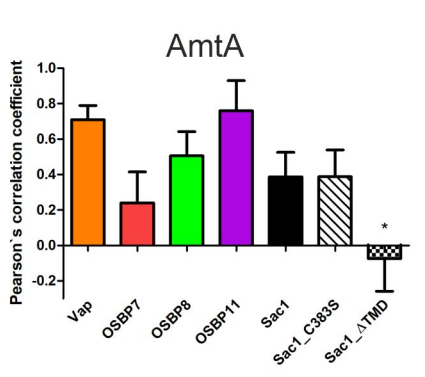
D
AmtA
Pearson`s correlation coefficient
1.0
0.8
0.6
0.4
0.2
0.0
-0.2
*
Vap
OSBP7
OSBP8
OSBP11
Sac1
Sac1_C383S
Sac1_ΔTMD

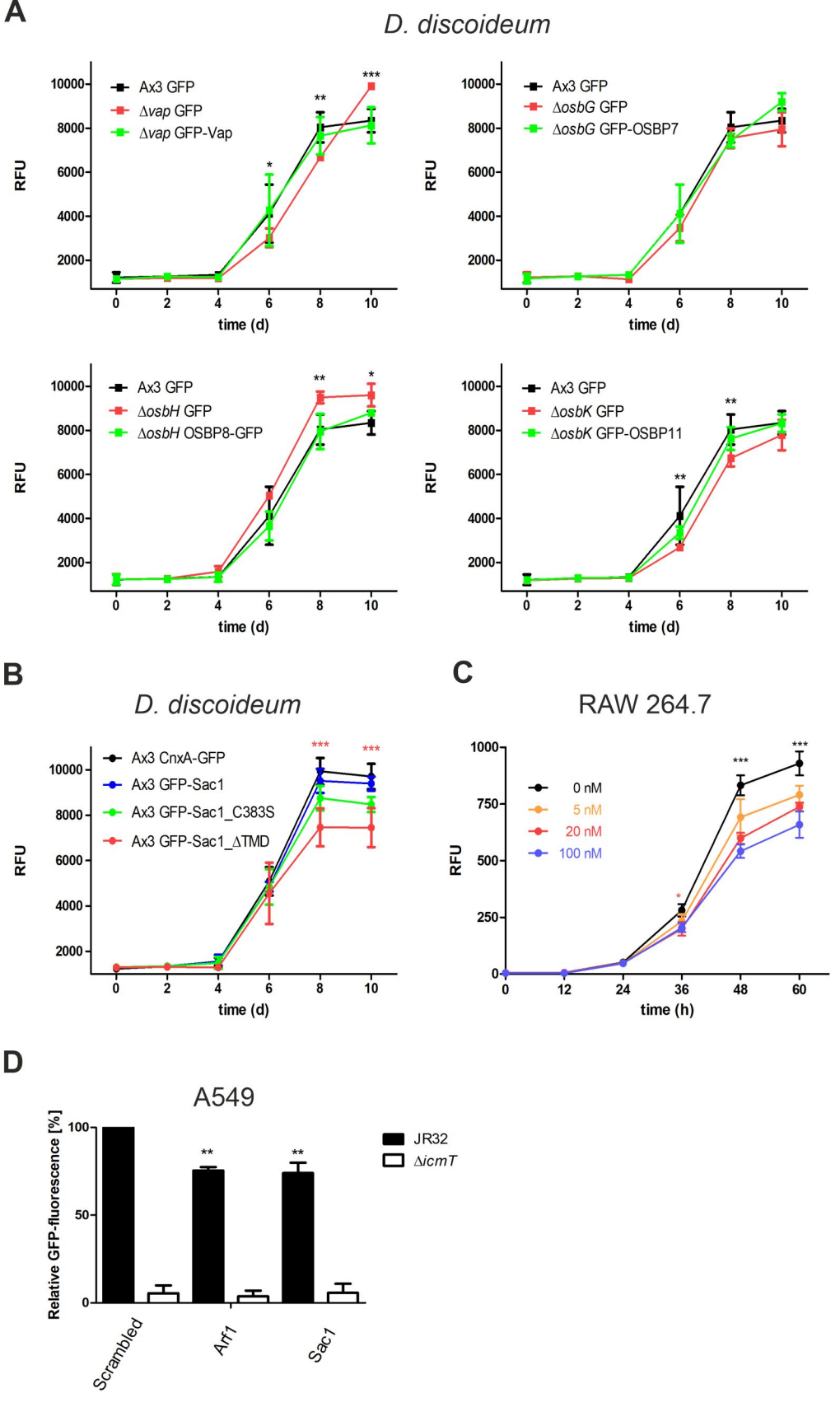
A
D. discoideum
Ax3 GFP
Δvap GFP
Δvap GFP-Vap
ΔosbG GFP
ΔosbG GFP-OSBP7
ΔosbH GFP
ΔosbH OSBP8-GFP
ΔosbK GFP
ΔosbK GFP-OSBP11
RFU
time (d)
B
D. discoideum
Ax3 CnxA-GFP
Ax3 GFP-Sac1
Ax3 GFP-Sac1_C383S
Ax3 GFP-Sac1_ΔTMD
C
RAW 264.7
0 nM
5 nM
20 nM
100 nM
time (h)
D
A549
JR32
ΔicmT
Relative GFP-fluorescence [%]
Scrambled
Arf1
Sac1

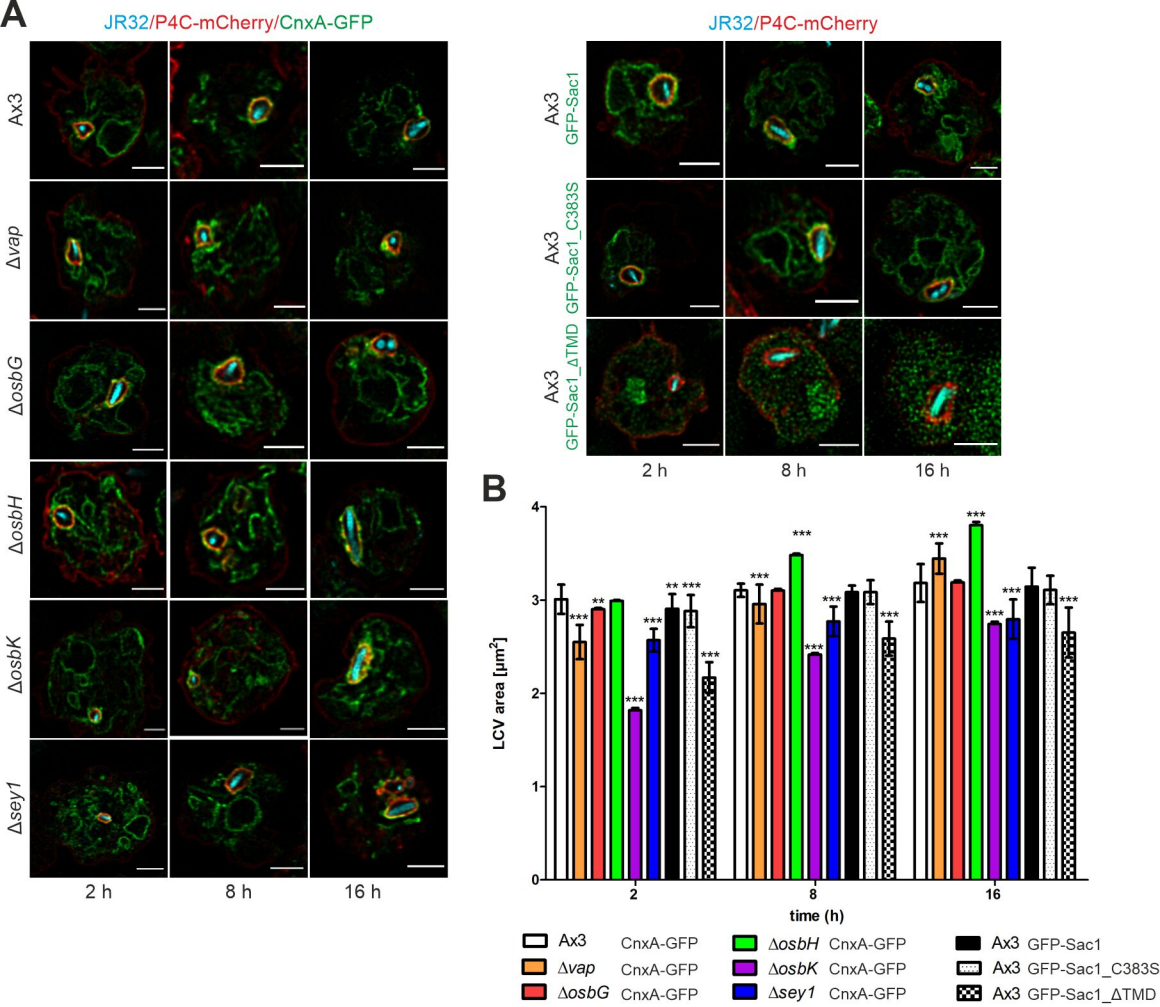
A
JR32/P4C-mCherry/CnxA-GFP
Ax3
Δvap
ΔosbG
ΔosbH
ΔosbK
Δsey1
2 h
8 h
16 h
JR32/P4C-mCherry
Ax3 GFP-Sac1
Ax3 GFP-Sac1_C383S
Ax3 GFP-Sac1_ΔTMD
2 h
8 h
16 h
B
LCV area [μm²]
time (h)
Ax3 CnxA-GFP
Δvap CnxA-GFP
ΔosbG CnxA-GFP
ΔosbH CnxA-GFP
ΔosbK CnxA-GFP
Δsey1 CnxA-GFP
Ax3 GFP-Sac1
Ax3 GFP-Sac1_C383S
Ax3 GFP-Sac1_ΔTMD

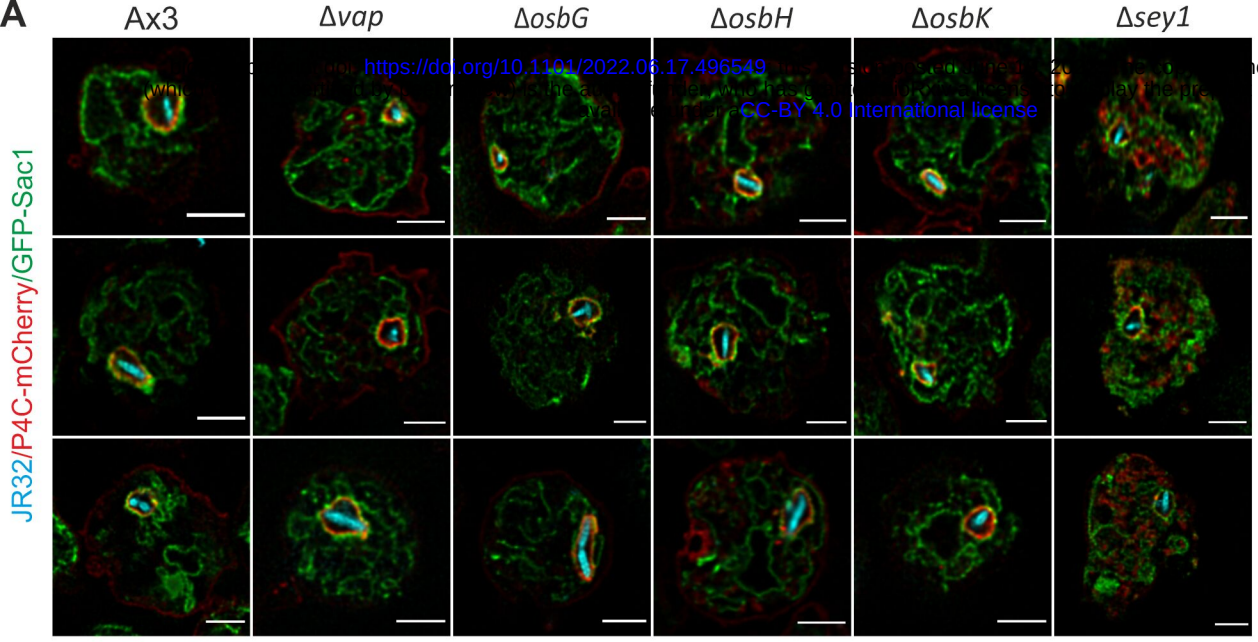

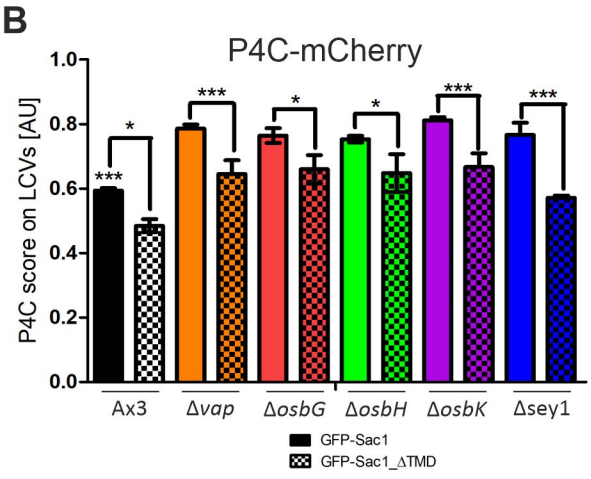

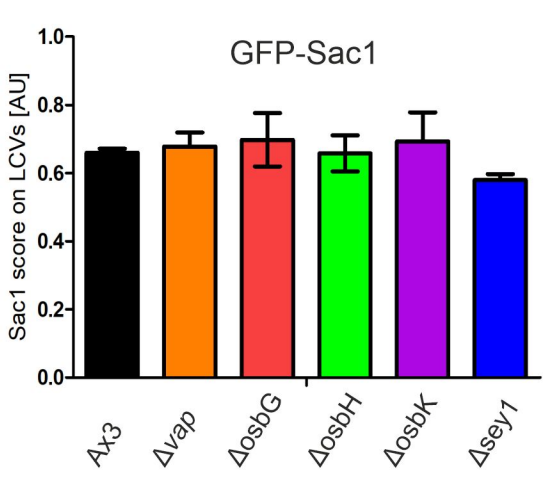

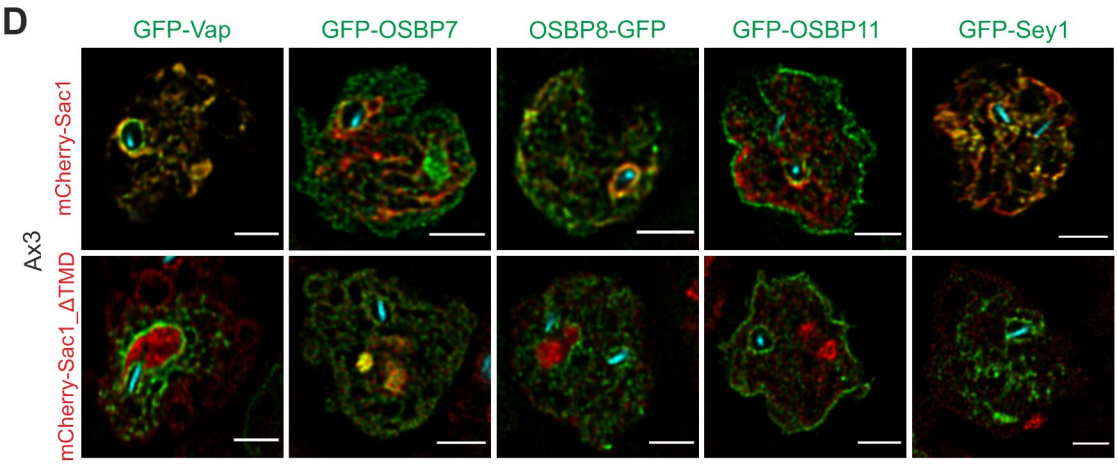

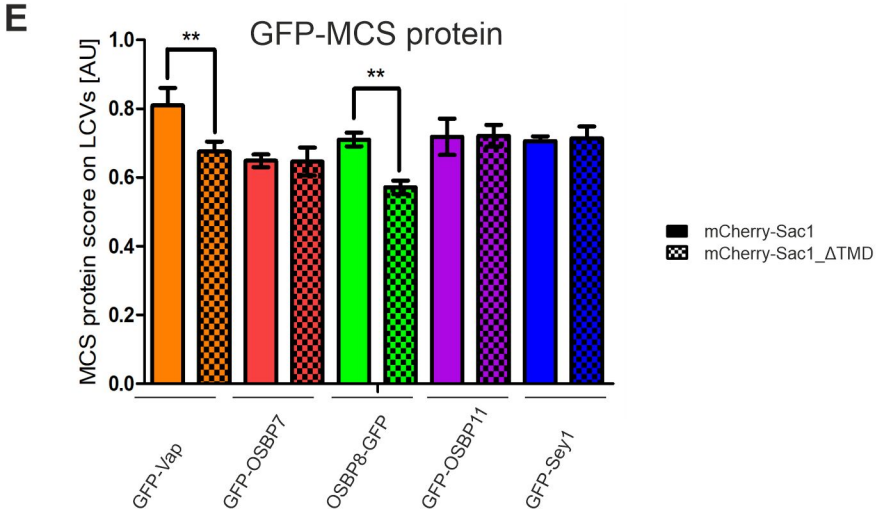

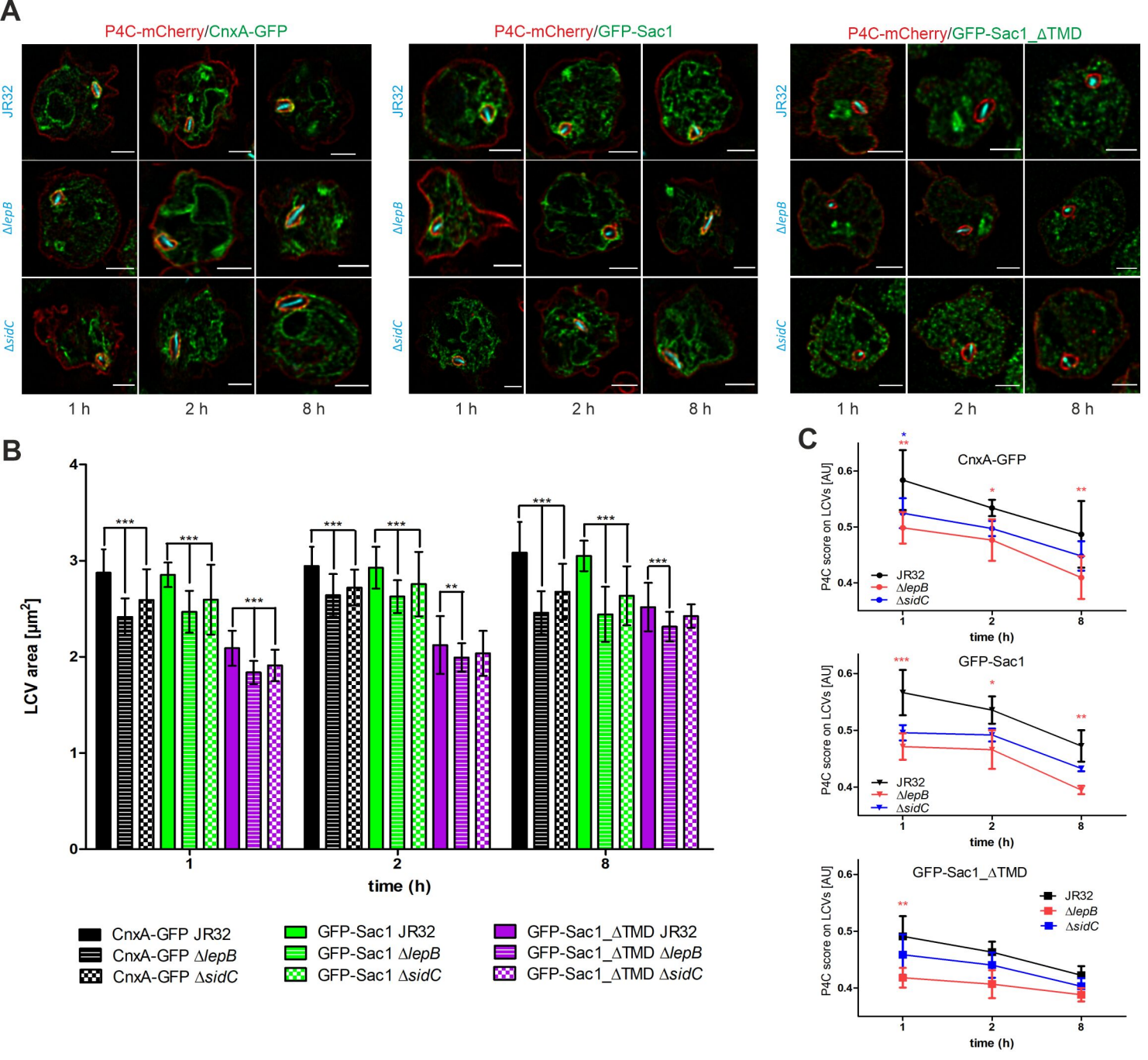
A
P4C-mCherry/CnxA-GFP
P4C-mCherry/GFP-Sac1
P4C-mCherry/GFP-Sac1_ΔTMD
JR32
ΔlepB
ΔsidC
1 h
2 h
8 h
B
LCV area [μm²]
time (h)
CnxA-GFP JR32
CnxA-GFP ΔlepB
CnxA-GFP ΔsidC
GFP-Sac1 JR32
GFP-Sac1 ΔlepB
GFP-Sac1 ΔsidC
GFP-Sac1_ΔTMD JR32
GFP-Sac1_ΔTMD ΔlepB
GFP-Sac1_ΔTMD ΔsidC
C
CnxA-GFP
GFP-Sac1
GFP-Sac1_ΔTMD
P4C score on LCVs [AU]
time (h)
JR32
ΔlepB
ΔsidC

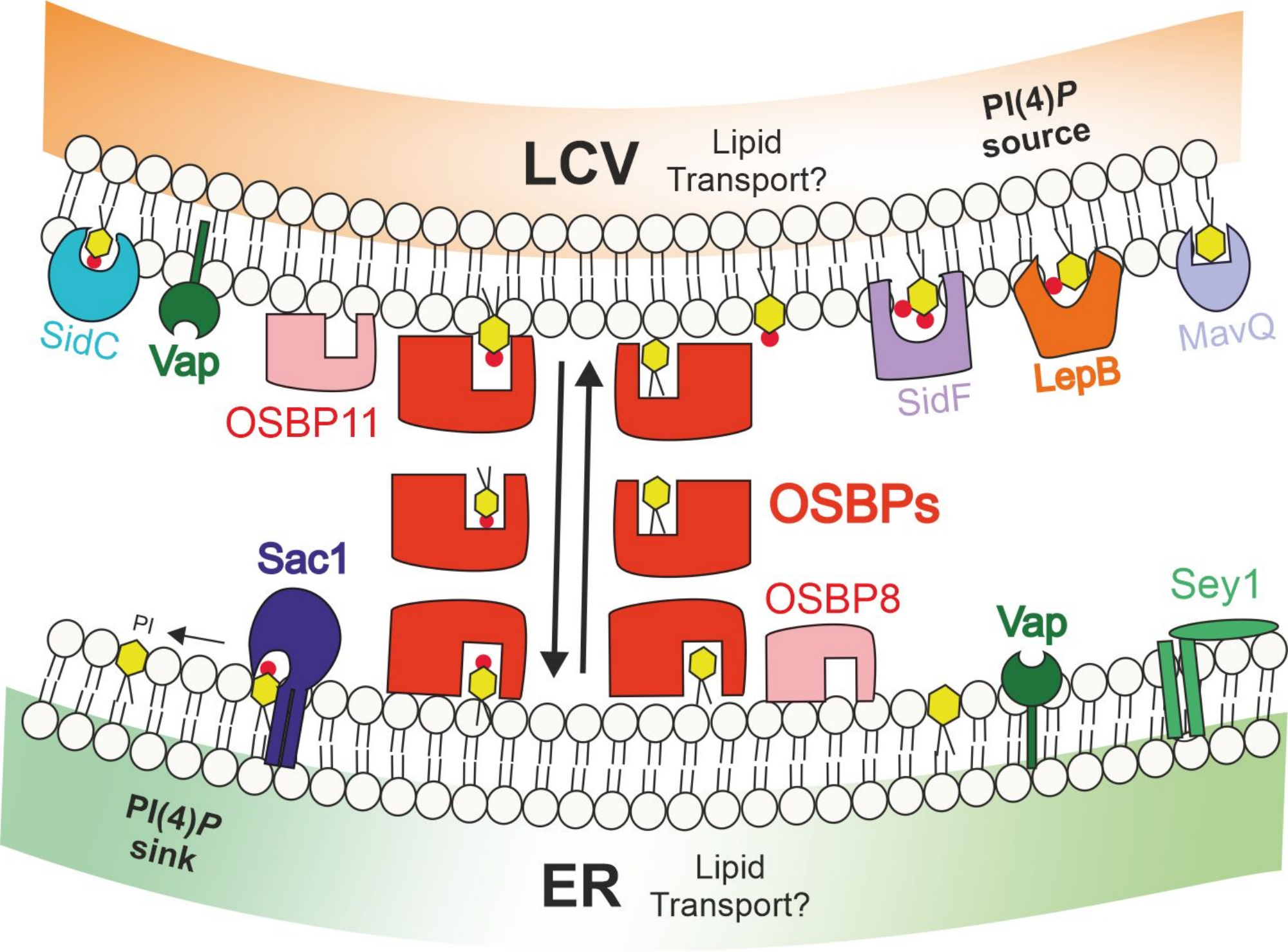
LCV
Lipid Transport?
PI(4)P source
SidC
Vap
OSBP11
SidF
LepB
MavQ
OSBPs
Sac1
OSBP8
Vap
Sey1
PI
PI(4)P sink
ER
Lipid Transport?